PUB-5400

Lawrence Berkeley Laboratory
UNIVERSITY OF CALIFORNIA

Accelerator & Fusion Research Division

EW20.0 Elliptical Wiggler Conceptual Design Report

ALS Insertion Device Group

March 1995

U. C. Lawrence Berkeley Laboratory
Library, Berkeley

FOR REFERENCE

Not to be taken from this room

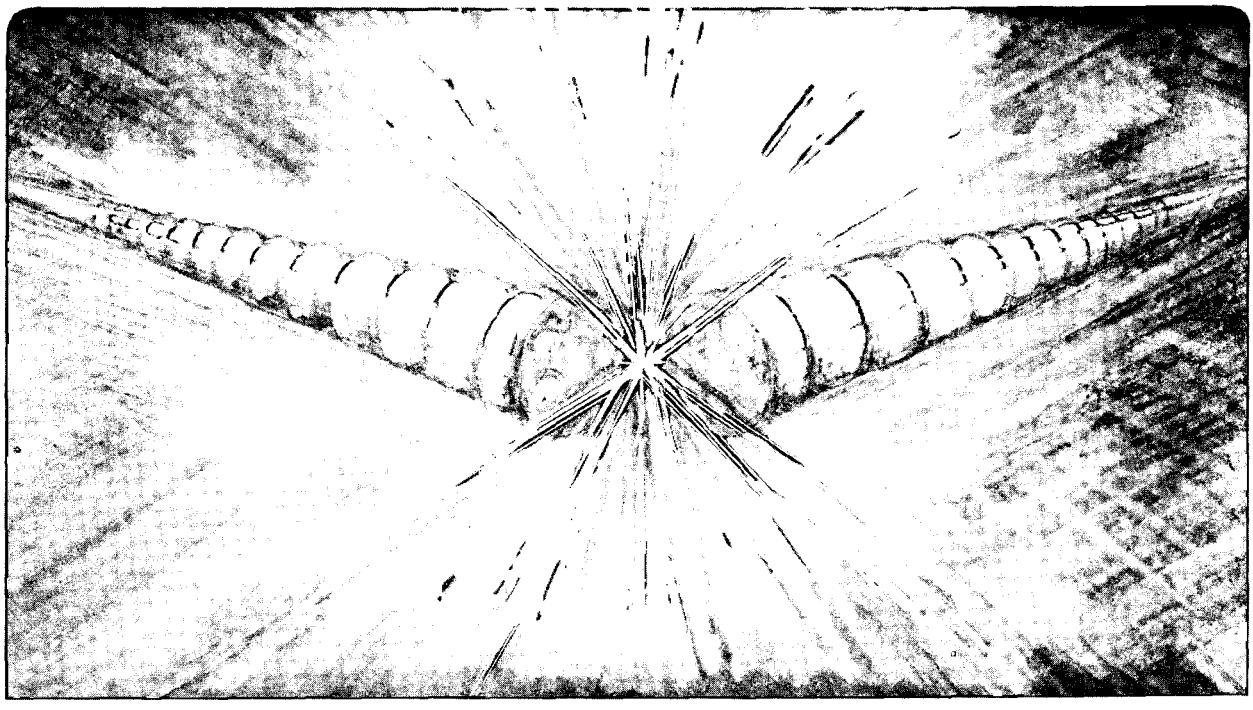

REFERENCE COPY
Does Not
Circulate
Copy 1
Bldg. 50 Library.
PUB-5400

Prepared for the U.S. Department of Energy under Contract Number DE-AC03-76SF00098

DISCLAIMER

This document was prepared as an account of work sponsored by the United States Government. While this document is believed to contain correct information, neither the United States Government nor any agency thereof, nor the Regents of the University of California, nor any of their employees, makes any warranty, express or implied, or assumes any legal responsibility for the accuracy, completeness, or usefulness of any information, apparatus, product, or process disclosed, or represents that its use would not infringe privately owned rights. Reference herein to any specific commercial product, process, or service by its trade name, trademark, manufacturer, or otherwise, does not necessarily constitute or imply its endorsement, recommendation, or favoring by the United States Government or any agency thereof, or the Regents of the University of California. The views and opinions of authors expressed herein do not necessarily state or reflect those of the United States Government or any agency thereof or the Regents of the University of California.

PUB-5400

EW20.0 Elliptical Wiggler Conceptual Design Report

ALS Insertion
Device Group

March 1995

Contents

Summary iii

1.0 Scope 1

2.0 Parameter Definition and Review Processes 3

2.1 Parameter Changes 3

2.2 Review Process 3

3.0 Insertion Device Performance 5

3.1 Principle of Operation 5

3.2 Spectral Requirements 5

3.3 Accelerator Requirements 7

4.0 Insertion Device Specifications 9

4.1 Magnetic Structure 9

4.1.1 Vertical Magnetic Structure Requirements 9
4.1.2 Requirements for CSEM Blocks 12
4.1.3 Backing Beam Requirements 13
4.1.4 Vertical End Structure Requirements 13
4.1.5 Axial Temperature Gradient 14
4.1.6 Horizontal Magnetic Structure Requirements 14

4.2 Magnetic Measurement Requirements 14

4.2.1 Block Measurements 14
4.2.2 Requirements For Measurements of the Full Insertion Devices 15

4.3 Vacuum System 16

4.3.1 Aperture Requirements 16
4.3.2 Vacuum Requirement 16
4.3.3 Diagnostics 16

5.0 Insertion Device Conceptual Design 17

5.1 Design Philosophy 18

5.2 Design Parameters 18

5.3 Vertical Magnetic Structure 20

5.3.1 Vertical Periodic Structure Magnetic Design. 20

5.3.1.1 Calculation of Structure 21
5.3.1.2 Harmonic Content of Wiggler Fields 22
5.3.1.3 Block Sorting 22
5.3.1.4 Sorting for Uniform Pole Excitation 22
5.3.1.5 Sorting for Reduced Integrated Field Errors 23

5.3.2 End Magnetic Structure Design 24

5.3.3 Multiple Trim Magnets 24
5.3.4 Vertical Periodic Magnetic Structure Mechanical Design 25
5.3.5 Vertical End Structure Mechanical Design 27
5.3.6 Multiple Trim Magnets Design 27
5.3.7 Field Error Corrections Design 27
5.3.8 Backing Beam Mechanical Design 27
5.3.9 Magnetic Structure Alignment 28

5.4 Horizontal Magnetic Structure 30

5.4.1 Horizontal Magnetic Structure Magnetic Design 30
5.4.2 Horizontal Magnetic Structure Mechanical Design 32
5.4.3 Horizontal Magnetic Structure Power Supply 32

5.5 ID Magnetic Measurement Facility 32

5.6 Support/Drive System 33

5.6.1 Support Structure Design 34
5.6.2 Mechanical Drive System Design 36
5.6.3 System Assembly 38
5.6.4 Local Temperature Control 38

5.7 Insertion Device Control System 38

5.8 Vacuum System 40

5.8.1 Vacuum Chamber 40
5.8.2 Pumping System Design 42
5.8.3 Insertion Device Vacuum Control and Diagnostics 42
5.8.4 Transitions 43
5.8.5 Vacuum Chamber and Pumping System Support 43

5.9 Installation 44

5.9.1 Vacuum chamber installation 44
5.9.2 Installation Preparation 44
5.9.3 Elliptical Wiggler installation into the Storage Ring 44

References 45

Summary

The EW20.0 Elliptical Wiggler described here is a cross-field device with a 20 cm period and a 3.5 m length. Designed for the Advanced Light Source (ALS), this insertion device will provide elliptically polarized light in the 50 eV–10 keV energy range with chirality switching up to 1 Hz.

This conceptual design report includes sections on: parameter development, spectral performance and accelerator requirements, physics specifications and the detailed conceptual design of the magnetic structure, the support/drive systems, the insertion device control system, the vacuum system, and installation for the EW20.0 Elliptical Wiggler.

1.0 Scope

The purpose of this conceptual design report is to assemble in a single document the preliminary design of the EW20.0 Elliptical Wiggler. This report describes the establishment of the parameters, the performance, the specifications, and the proposed design. Adoption of this conceptual design report will provide a baseline design from which a detailed design of the EW20.0 Elliptical Wiggler can follow.

Specifically, the sections of this conceptual design report include:

Section	Description
2.0	PARAMETER DEFINITION AND REVIEW PROCESSES—How the EW20.0 parameters were established, how they can be changed, and the planned review process to insure an acceptable design.
3.0	INSERTION DEVICE PERFORMANCE—EW20.0 Spectral performance and accelerator requirements.
4.0	INSERTION DEVICE SPECIFICATIONS—EW20.0 Physics and the magnetic measurement specifications.
5.0	INSERTION DEVICE CONCEPTUAL DESIGN—Detailed conceptual design descriptions of the subsystems of the EW20.0 Elliptical Wiggler. The subsystems include:

Section	Subsystem
5.1	Design Philosophy
5.2	Design Parameters
5.3	Magnetic Structure
5.4	Insertion Device Magnetic Measurement Facility
5.5	Support/Drive System
5.6	Insertion Device Control System
5.7	Vacuum System
5.8	Installation

The cost estimate and the associated fabrication schedules for the EW20.0 Elliptical Wiggler are found elsewhere.[1]

2.0 Parameter Definition and Review Processes

The parameters for the insertion device for the ALS are determined from a broad range of requirements that have been evolving since the Advanced Light Source was first proposed in 1982. However, there are 3 major areas that combine to establish the ID parameters. These are:

- Spectral requirements—as proposed by the potential users of the ALS,
- Accelerator design—as developed by the ALS Accelerator Physics and Engineering Groups,
- Performance and tolerance limits for the mechanical, magnetic, and electrical components—as developed by the ALS Experimental Systems and Engineering Groups.

2.1 Parameter Changes

Following the conceptual design review, this document will be updated and will establish the baseline EW20.0 Elliptical Wiggler design parameters. To change the parameters after this point in the process will require a formal review of the proposed changes along with an assessment of the impact the changes will have on device performance, cost, and schedules. Parameter changes are initiated by submitting a proposed change on an ALS Parameter List/Scope Change Authorization Form; submitting it to the Planning and Development Group. To be approved, the proposed change must be reviewed by the following three groups: Accelerator Physics, Experimental Systems, and Engineering.

2.2 Review Process

Adoption of this conceptual design report establishes a baseline conceptual design for the EW20.0 Elliptical Wiggler. The follow-on to this conceptual design is the detailed design of the various subsystems and the respective final design reviews of these subsystems prior to commencing fabrication.

For the EW20.0 Elliptical Wiggler, some of the subsystem designs are very similar to those of the already completed U8.0 Undulator so final design reviews are not planned.[2]

3.0 Insertion Device Performance

3.1 Principle of Operation

With a conventional wiggler, the radiation from each individual pole behaves qualitatively like that from a bend magnet. On the horizontal midplane the flux is linearly polarized (i.e., the degree of circular polarization is zero). As the observer moves vertically off axis, the absolute value of the degree of circular polarization increases. The degree of circular polarization above the midplane is of opposite handedness as that below the midplane. This provides the basis for the observation of circularly polarized flux from bend magnets. However, the radiation from a series of wiggler poles, viewed off axis, exhibits no net circular polarization, since it consists of the radiation from poles of alternating polarity, which produce radiation of alternating chirality. Circularly polarized flux, similar in quality to that from a bend magnet, can be produced on the midplane through the use of a periodic horizontal magnetic field, shifted spatially 90 degrees relative to the vertical field. The horizontal field deflects the electron beam vertically as it passes through the vertical field and provides an effect on axis which is equivalent to viewing the radiation from successive poles first from above the midplane and then from below. This is schematically illustrated in FIG. 1.

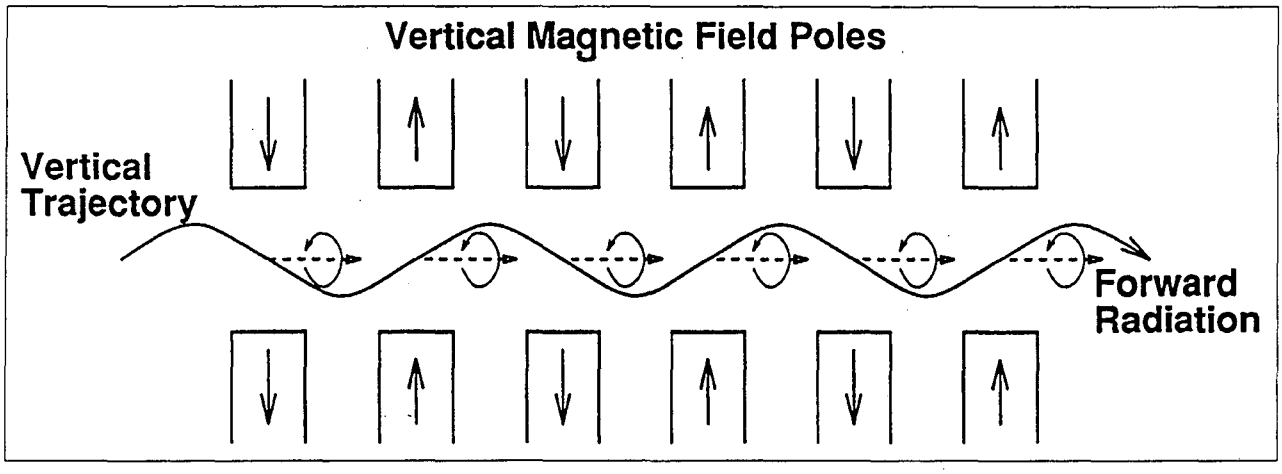

FIG. 1. Elliptical Wiggler schematic of operation.

3.2 Spectral Requirements

The EW20.0 Elliptical Wiggler will be the second ALS wiggler—specifically designed to deliver high-intensity circularly polarized flux. The device consists of periodic vertical and horizontal magnetic structures. The vertical magnetic structure is a hybrid permanent magnet design, similar to other ALS insertion devices. The horizontal magnetic structure is an electromagnet; this provides the vertical deflection necessary for production of circularly polarized flux.

The device will be 3.4 m long, consisting of 14 periods, with a 20 cm period length. It is designed to operate in the energy range of 50–10000 eV. The wiggler will supply radiation to 2 beamlines: a low energy beamline using a grating monochromators that will operate below 2,000 eV and a high-energy beamline with a crystal monochromator that will operate above 2,000 eV. The horizontal radiation fan must be at least 10 mrads to allow the possibility of a beam-splitting arrangement to simultaneously fill both beamlines.

The spectral output of an elliptical wiggler involves a trade-off between flux density and degree of circular polarization.[3] As the vertical deflection is increased, the degree of circular polarization increases, but the flux density decreases. For this reason, the optimization of the output circularly polarized flux must consider an appropriate combination of the two parameters. For many experiments, where experimental noise is statistical in nature, the appropriate figure of merit, M, is

$$M = P_c^2 \frac{d^2F}{d\Omega}$$

where P_c is the degree of circular polarization, and $d^2F/d\Omega$ is flux density. To maximize M over the range of

energies, the peak vertical field strength is varied by changing the vertical magnetic gap, and the vertical deflection is varied by changing the current in the horizontal magnetic structure. The maximum peak vertical field is 2.0 T, and the maximum deflection parameter, K_x associated with the horizontal field is 1.5. The deflection parameter is defined as

$$K_x = \Sigma(-1)^{\frac{(n+1)}{2}} \frac{B_{xn}}{n}; \quad n = 1, 2, 3...$$

where B_{xn} are the cosine field components.

Tables I and II show optimum settings for electron energies of 1.5 and 1.9 GeV, respectively. FIG. 2 provides a summary of the elliptical wiggler spectral performance for the ALS operating at 400 mA, for 1.5 GeV and 1.9 GeV electron energies, and for a fixed 5 mrad horizontal aperture centered about the axis. The figure is a plot of optimized M vs. photon energy.

Table I. Optimization for 1.5 GeV electron energy.

Photon Energy (eV)	Peak Vertical Field (T)	Vertical Deflection Parameter	Vertical Half-aperture (mrad)	Integrated Merit Function 10^{13} Photon/Sec
50	0.4	1.5	0.333	3.49
		1.83	0.305	3.49
100	0.5	1.49	0.256	3.65
150	0.5	1.30	0.229	3.65
300	0.8	1.13	0.220	3.66
700	1.6	1.07	0.212	3.59
1000	2.0	1.02	0.191	3.38
1500	2.0	0.88	0.165	2.94
3000	2.0	0.68	0.127	1.77
7000	2.0	0.48	0.091	0.415
10000	2.0	0.42	0.079	0.139

Table II. Optimization for 1.9 GeV electron energy.

Photon Energy (eV)	Peak Vertical Field (T)	Vertical Deflection Parameter	Vertical Half-aperture (mrad)	Integrated Merit Function 10^{13} Photon/Sec
5.0	0.5	1.5	0.391	3.90
		2.34	0.317	3.96
100	0.5	1.5	0.283	4.40
		1.83	0.261	4.40
150	0.6	1.5	0.243	4.57
		1.64	0.231	4.57
300	0.7	1.33	0.190	4.62
700	1.1	1.12	0.174	4.63
1000	1.4	1.07	0.170	4.59
1500	2.0	1.04	0.154	4.33
3000	2.0	0.80	0.119	3.28
7000	2.0	0.58	0.086	1.34
10000	2.0	0.51	0.075	0.668

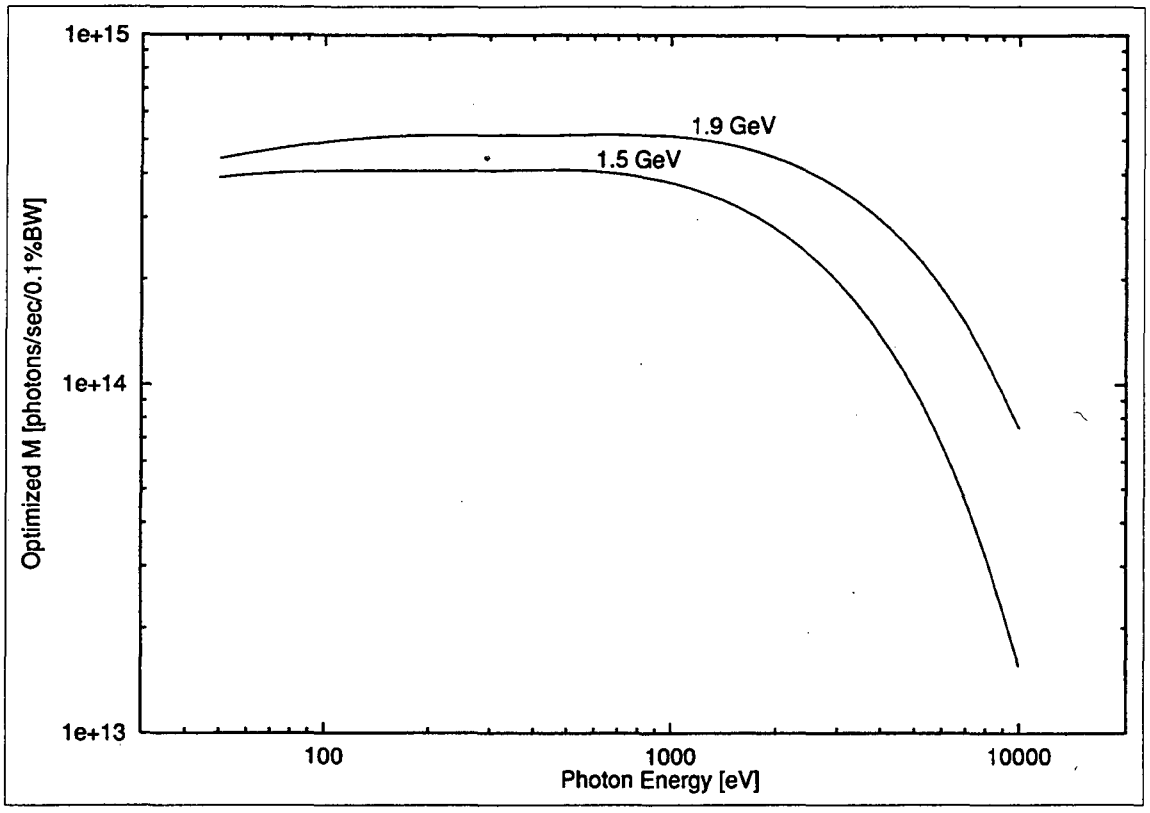

FIG. 2 Elliptical Wiggler performance.

3.3 Accelerator Requirements

The beam in the accelerator is affected in two general ways by the magnetic fields in the insertion devices. The first is associated with the fields expected in a perfect device and the second with the possible error fields. In addition, the electrons will interact with any ions trapped in the combined fields of the electron beam and the insertion devices. Each of these items must be addressed in the process of insertion device design.

In a perfect device, the periodic fields produce focusing in the vertical plane of the storage ring. For electrons in the core of the beam, this focusing requires minor adjustments of the strengths of the storage ring quadrupoles. However, this focusing causes a break in the natural periodicity of the magnet lattice, which leads to a reduction of the dynamic aperture. Further, the higher spatial harmonics intrinsic to the perfect device contribute to perturbing forces that limit the momentum acceptance of the storage ring. Both these effects lead to a reduction of beam lifetime.

These phenomena have been studied by the Accelerator Systems Group using tracking codes. They concluded that the effects of insertion devices (operating at their maximum fields) on the dynamic aperture of an otherwise perfect machine, were substantial. However, the machine acceptance, which determines the gas scattering lifetime, was limited by the vacuum chamber gap in the insertion device itself, not by the reduction in dynamic aperture. When other machine imperfections were considered, an unexpected phenomenon was observed, causing a reduction in the Touschek lifetime. This effect is still under investigation. However, the results to date indicate that the resulting beam lifetime, including the effects of both insertion devices and the machine imperfections, will be acceptable.

The fact that the insertion devices have an effect on the machine must be balanced against other effects inherent in a real machine. For example, if the field errors in the ring accelerator magnets are considered alone, there is a significant decrease in the dynamic aperture. The effects of both have been calculated and the expectation at present is that insertion devices meeting the proposed specifications will not cause noticeable degradation of the dynamic aperture of the ALS beyond that produced by other errors.

Error fields are introduced by construction tolerances, as well as by the intrinsic fields of the insertion devices. The main problem with these field components, as far as the storage ring is concerned, is that they change as the undulator field changes. Correction elements that compensate for the linear terms are included in the machine. To compensate for the effects of each scanning device simultaneously will require action by the control system. Therefore, specifications are developed for the error fields that will have a minimal effect on the storage ring, possibly without the necessity for compensation over a range of insertion device gaps.

The first and second integrals of the principal field, B_y, should be zero for all values of the gap. Non-zero integrals will lead to an electron beam horizontal displacement in the insertion device and a net horizontal kick. One of the most significant effects of vertical error field will be horizontal distortions of the electron orbit at other places around the ring. These distortions can be significantly larger than the displacements in the device and can have a significant effect on the performance of other insertion devices and their experimental beam lines. The limit set on the vertical field integral is 100 G cm.

Likewise, the first and second integrals of the field orienting the local beam axis (B_x) should be zero for all values of gap. Non-zero integrals will lead to an electron beam vertical displacement in the insertion device and a net vertical kick. Additionally, there will be some horizontal magnetic fields perpendicular to the beam in the device due to various errors associated with horizontal and vertical magnetic structures. These fields are not easily calculable, but their limit can be set based on steering requirements at a somewhat higher level, 500 G cm. They will be corrected by the ALS steering magnets.

The above values are relatively small, but within the range of measurements that have been made for the other devices built and measured by Lawrence Berkeley Laboratory.

In addition to net dipole fields in the devices, there is the need to assure that off-axis particles are not focused by integrated fields in the device, and that the beam will not be steered incorrectly if it does not pass exactly down the center. These requirements establish the limits on the allowable quadrupole, skew quadrupole, and sextupole. These are presently set at 100 G cm/cm, 100 G cm/cm, and 100 G cm/cm^2, respectively. Furthermore, so as not to degrade beam lifetime, field integrals must remain relatively uniform over the entire ± 1 cm vertical by ± 3 cm horizontal "good field region," which extends outside the convergence radius for expansion in multipoles. Integrated fields and gradients everywhere in this region should not exceed 100 G cm and 100 G cm/cm, respectively.

There are questions associated with the commissioning of the machine that affect the insertion devices. To achieve a high magnetic field in the devices, it is necessary to have the gap as small as possible. For both commissioning and normal operation, we have chosen 1.4 cm as the minimum vertical gap, which corresponds to a vacuum chamber aperture of 1.0 cm.

The machine requirements placed on the insertion device are summarized in Table III, including the vacuum requirement of 10^{-9} Torr, which is typical of the entire machine.

TABLE III. Requirements on the ALS insertion devices.

Parameter	Limit
$\int B_y \, dl$	100 G cm
$\iint B_y \, ds \, dl$	100 G cm^2
$\int B_x \, dl$	500 G cm
Integrated quadrupole	100 G cm/cm
Integrated skew quadrupole	100 G cm/cm
Integrated sextupole	100 G cm/cm^2
Required vacuum	10^{-9} Torr

4.0 Insertion Device Specifications

4.1 Magnetic Structure

The EW20.0 Elliptical Wiggler will incorporate a vertical hybrid-magnetic structure consisting of Nd-Fe-B magnetic blocks and vanadium permendur poles and a horizontal iron-core electromagnet structure consisting of laminated iron pole pieces surrounded by copper coils. The hybrid is chosen because it has several advantages over the pure current sheet-equivalent material (CSEM) design.

- The field is dominated by the characteristics of the poles, which can be made uniform both in size and magnetic performance.
- The errors in magnetic moments of the blocks can be averaged by sorting the blocks for the poles.
- Errors in the total magnetic moment of all the blocks on a pole have little effect on the electron beam, or the spectrum—because they contribute equally to adjacent poles and produce no electron beam steering.
- The peak field at each pole can be tuned by a small amount.
- A higher peak field is achievable at small gap/period ratios.

The iron-core electromagnet, which serves to bend the local beam-axis alternately up, then down each period, is chosen to provide 1 Hz cycling of polarization polarities. Again, the horizontal field is dominated by the characteristics of the iron rather than by the coil, leading to uniformly-periodic magnetic fields.

4.1.1 Vertical Magnetic Structure Requirements

The engineering tolerances for construction of the EW20.0 Elliptical Wiggler for the ALS are based on the design performance of the device as installed.

The effect of the integrated fields on the electron beam are most important. As mentioned above, the integrated dipole must be held to less than 100 G cm. This will be accomplished by:

(a) sorting the PM blocks so as to uniformly energize poles and minimize block minor component effects,
(b) designing the ends to have as small a dipole effect over the range of gaps as possible,
(c) utilizing tunable trim magnets on end poles,
(d) employing an even number of vertical poles,
(e) implementing multiple trim magnets, which have been used quite successfully on IDA, IDB, and IDC,
(f) using the external corrector magnets as needed.

Integrated quadrupole can be produced by poles that are titled to the midplane and by PM block errors and non-uniformity.

Considering the pole tilt alone, the magnitude of the allowable tilt angle α (radians), if there were no correction capability, is given by:

$$\alpha = \frac{4h\sigma_q}{\sqrt{N}\lambda B_{pole}}$$

where N is the number of periods, h is the half gap, where l is the period, and σ_q is the acceptable integrated quadrupole 100 G-cm/cm. This calculation gives an allowable pole tilt of about 175 μradians, or 14 μm, across the width of the pole. It may be difficult to achieve this accuracy, so a tolerance similar to the ALS undulators, (i.e., 30 μm) will be assigned, and multiple trim magnets will be employed to reduce the residual integrated quadrupole, if necessary.

The effects of the random errors are determined by a set of calculations that are based on the hybrid CSEM insertion device theory developed by K. Halbach.[4] Possible errors, shown in FIG. 3, include vertical motion of a pole, variations in pole thickness, misorientation of the CSEM's easy axis near the electron beam, and different spacings between the two poles and the CSEM block in a half period. In this section, we generate the values for the engineering tolerances for EW20.0 from the error calculations.[5,6] The magnitude of each error, mentioned above, which will produce a 0.1% variation (σ) in the integrated flux crossing the midplane, per single half period, is given in Table IV.

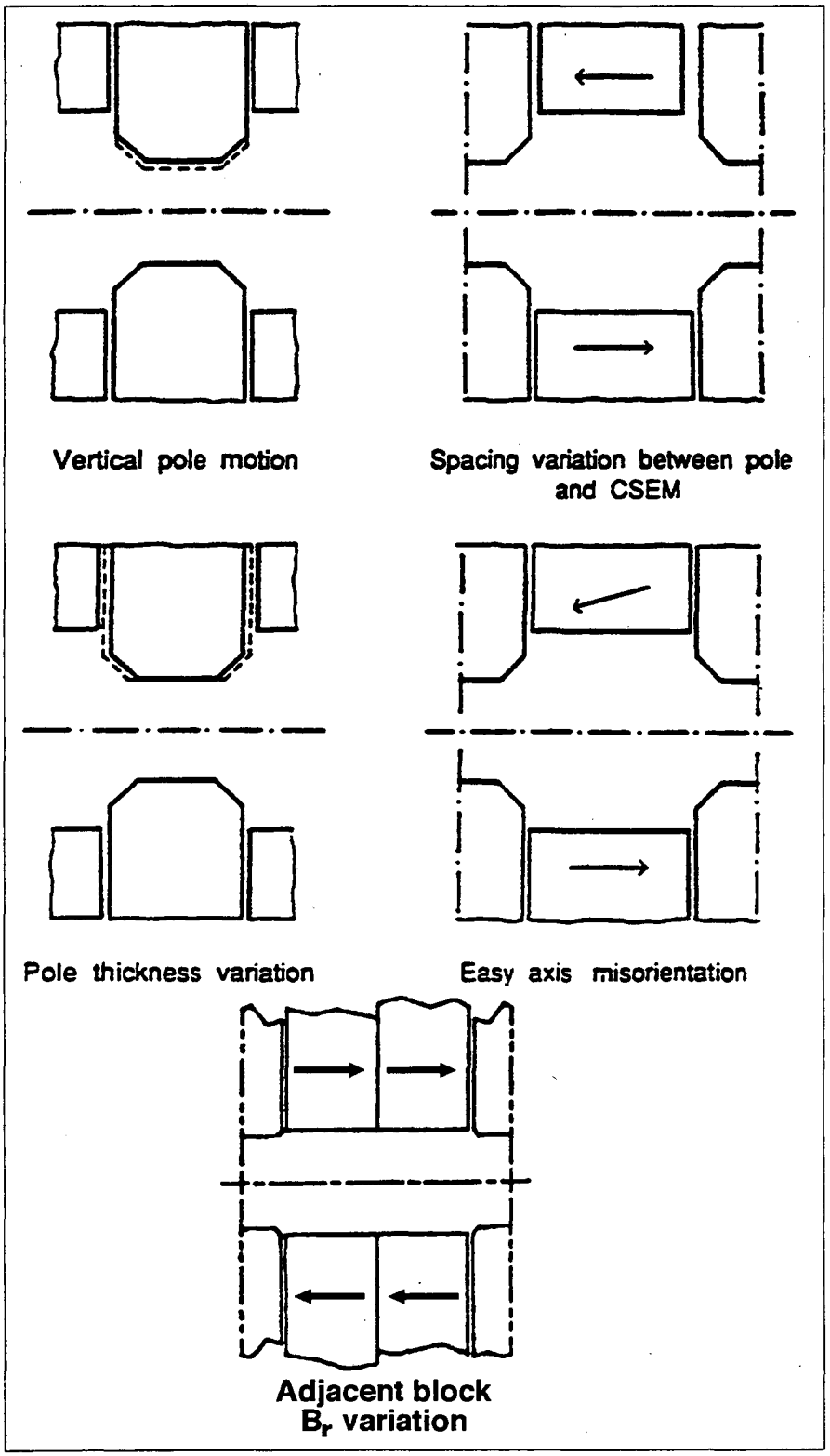

FIG. 3. Hybrid magnetic structure errors.

In addition to these errors, there is the possibility of an error in the wiggler that is not possible in the ALS undulators. It is due to the long period and the need to have blocks on both sides of the poles, or equivalently, two blocks along the axial direction between poles. Where these blocks contact, there will be—in effect—2

surfaces of magnetic charge. If the strengths B_r of the 2 blocks are identical, there will be no effect on the beam. If different, then the beam can be deflected. A 0.1% variation can be caused by a ΔB_r of 1.2%.

TABLE IV. Summary of individual errors that produce a 0.1% variation (s) in the integrated flux across the midplane for the EW20.0 magnetic design gap of 1.40 cm.

Error Type	EW20.0 Value
Vertical pole motion	21 μm
Pole thickness	430 μm
Easy-axis orientation (closest block to beam)	1.28 degrees
Spacing variation between poles and CSEM	196 μm
Variation of B_r in two adjacent blocks	136 Gauss

It is necessary, for the purpose of building a device, to discuss the limits in the form of mechanical tolerances rather than errors. The relation between an error σ and a mechanical tolerance can be determined by assuming a uniform distribution of any parameter within the tolerance *t*, and requiring that the mean square variation be the equivalent to that of a Gaussian. The conclusion is that a tolerance *t* should be about 1.73 times the equivalent error σ based on a Gaussian distribution.

Of the several errors to be considered, there are 2—the CSEM centering error and the pole width error—that are easy to control. These are addressed first, followed by the pole position error, which is determined by machine requirements, and the remaining error allowance is used to determine the maximum allowable easy-axis orientation error and the B_r variation in the Nd-Fe-B blocks.

The variation in the spacing between the CSEM and each side of the poles is determined by the tolerance buildup of poles, CSEM, and holder. It is possible to ascribe a maintainable tolerance of 100 μm to this difference, corresponding to a σ of 60 μm, or 0.03%, which will be combined with the other errors.

The pole thickness can easily be controlled to 50 μm, which leads to a σ of 30 μm or $\leq$ 0.01%.

The error tolerance on vertical pole position is determined by two considerations. The first being the limit on quadrupole field in the insertion device, the second is the random field error at the midplane.

Pole tilt can introduce quadrupole fields. The effect of pole tilt on the random field error is small, but the maximum allowable quadrupole field limits the relative tilt of a pair of poles to 30 μm over the width of the 8 cm pole. Using this same value as the tolerance for the gap variation, the random error contribution will be 0.09%.

There can be errors in pole width. Using an approach similar to the one used with pole thickness errors, the pole width tolerance is 100 μm, which contributes little to the total error.

A major error is associated with misorientation of the easy axis. Having determined the other errors, the vertical easy-axis orientation error could be allowed to reach 3.0 degrees, thus, contributing 0.14% to the error budget. Nonetheless, those blocks centered just above or below the axis will be those with the smallest easy-axis orientation errors (< 3 degrees).

As for the permanent magnet strength mismatched for adjacent blocks, this will be limited to 200 Gauss, which gives rise to a 0.09% contribution to the error budget.

The error types, assigned tolerances, and magnetic field error contributions (σ) for the EW20.0 Elliptical Wiggler are summarized in Table V.

Table V. Summary of magnetic tolerances for the EW20.0 Undulator.

Error Type	Total Tolerance	Error (%)
Spacing CSEM to pole	100 μm	0.03
Pole thickness	50 μm	0.01
Vertical pole motion (gap)	26 μm	0.09
Easy-axis orientation	± 3 degree	0.14
Variation of B_r in adjacent blocks	200 Gauss	0.09
	Total:	**0.19**

Taken together, the error contributions above are negligible with regard to the wiggler's beamline performance. Achieving the practical tolerances above will minimize the integrated fields through the device which have to be corrected at wiggler ends.

The elliptical wiggler must also meet entrance and exit pole requirements. A total of 2 periods are sacrificed to provide appropriate steering and displacement over a range of gaps, and additionally, match the end excitement of the horizontal structures so as not to add a linear polarization contribution from the ends.

EW20.0 has a much larger wiggle amplitude (400 μm) than does U5.0 (11.4 μm), or even U10.0 (50 μm), and thus, through the ID, a larger horizontal offset from the nominal (unperturbed) beam axis were the ends to be configured with pole scalar potentials of 0, +1/2, -1, +1, etc. For scanning experiments, it is desirable to have horizontal beam position stable while changing the gap. Therefore, EW20.0 is designed with a 0, +1/4, -3/4, +1, -1, etc., scalar potential end configuration making average beam displacement through the insertion device zero with respect to the nominal beam axis. This excitation is made as gap-independent as possible. It also matches the horizontal structure end taper.

Unlike the ALS U5.0 and U8.0 devices, the EW20.0 will feature an even number of poles. This is to cancel the integrated sextupole-like component that comes from the ends of the device, and which affects particle trajectories parallel to the nominal beam axis.

Spectral performance of the first 3 ALS undulators (2 U5.0s and a U8.0) easily meets specifications. Integrated multipole fields initially did not meet accelerator requirements. Superposition of nonrandom, easy-axis orientation errors of blocks positioned transversely off center was a major cause. Needed correction was provided by sets of multiple trim magnets situated at both upstream and downstream undulator ends. Both normal and skew-integrated fields over the entire ± 1 cm by ± 3 cm "good field region" were corrected to within tightened specifications, which included gradient limits outside the multipole convergence radius. Additionally, these trim magnet arrays provided for correction of the linear component of integrated field gradients for particles with trajectories not parallel to the nominal beam axis. EW20.0 permanent magnet block sorting will reduce the above mentioned integrated field error source. Still, EW20.0 may make use of convenient multiple trim magnet arrays at undulator ends to further reduce these integrated fields.

The final set of parameters for the insertion device conceptual design are given in Section 5.2, Table VII.

4.1.2 Requirements for CSEM Blocks

Two types of blocks have been considered for the EW20.0 insertion device, samarium cobalt (Sm-Co) and neodymium iron boron (Nd-Fe-B). The advantage of Sm-Co is its high resistance to radiation, whereas Nd-Fe-B is a higher performance material. Because the EW20.0 can be expected to operate on the ALS for as long as 20 years, it was necessary to assess the possible effects of radiation over this period of time on these materials. A complete evaluation of this topic for the ALS insertion devices is given elsewhere.[7] The conclusions are summarized here.

The expected ionizing radiation in each ALS insertion device, based on the assumption that half the beam is lost during each fill in 5 of the insertion devices, and that there are 1,000 fills of the ALS per year, is only 3×10^6 rads. The limited data on Nd-Fe-B suggest that this level of radiation is below the level where there is a

detectable effect on the material performance. The effect expected from neutron radiation during the 20 year life of a device is even less.

During this study, there was an evaluation of the effect of shielding of the insertion device by the vacuum chamber. Both aluminum and stainless steel have been used successfully for this type of vacuum chamber. The aluminum chamber is less expensive and has better thermal conductivity. However, because the stainless steel has a higher density and a higher atomic number Z, it was thought that it might provide better shielding. A study using the EGS4 code was carried out at SLAC and the results show that there is little difference in this regard between aluminum and stainless steel. More importantly, the eddy currents induced in the vacuum chamber by the horizontal field electromagnets cycling at up to 1 Hz must not give rise to significant field errors. This requirement drives the vacuum chamber material choice and design.

The three components of magnetic moment are measured for all CSEM blocks before installation into the magnetic structure of an insertion device. Measurements are then used in a two-stage sorting process to arrange the blocks within the magnetic structure. The first-stage sort are based on values of the principal moment, which is aligned with the block's easy-axis, to achieve uniform pole excitation. The second stage considers the two minor components, which represents easy-axis orientation errors, to achieve uniform lateral field distribution.

Construction of the first three ALS insertion devices used only first-stage sorting. This clearly demonstrated the effectiveness of sorting to achieve uniform excitation. However, these first devices did exhibit a considerable integrated lateral field non-uniformity. The second stage sort has been added to correct this. Simulations show that this should be very effective.[8]

The Nd-Fe-B material used in the blocks must be of high quality. A coercive force, H_c, greater than 10.6 kOe, is specified. The magnetization must also be linear, to 120% of H_c (third quadrant) at a temperature of 50 degree C after thermal stabilization.

The block dimensions are determined by a complete magnetic analysis of the structure and are developed in Section 5.3.1. However, dimensional tolerances for the blocks are determined by: assembly procedures, overall tolerances of the set of blocks as they are bonded into the pole assembly, and the final assembly of the device. These considerations allow a dimensional tolerance of 60 μm for the block thickness.

The variation of the dipole moment of the individual blocks is determined by an assigned 0.1% standard deviation allowed in the total magnetization on the poles.

The Nd-Fe-B blocks must also be supplied with appropriate surface preparation for good adhesion in the pole/keeper assembly, and to avoid oxidation over the expected life of the device.

4.1.3 Backing Beam Requirements

The spectral width of the output of an undulator is determined by the following factors:
- the intrinsic linewidth;
- the momentum spread of the electron beam;
- the angular divergence of the electron beam;
- the systematic variation of gap along the insertion device.

The first of these is determined by the insertion device design. The next 2 depend on the machine and its operating conditions. The last item is determined, to first order, by the structural rigidity of the device and the temperature gradients in the structure, which lead to gap variations. The output of a wiggler on a machine such as the ALS is relatively insensitive to all 4 of these variations. Therefore, flexing of the backing beam due to the magnetic load is not expected to affect performance. However, the backing beam must have some rigidity, and must provide a support system for the ALS insertion device magnetic field measuring system. A recommended approach is to simply use the same cross section for the baking beam as was used for the U5.O and U8.0 Undulator backing beams.

4.1.4 Vertical End Structure Requirements

Field correction capability will be built into the last energized pole pair at each end of the insertion device The purpose of these corrections is to provide correct entry and exit of the electron beam and to allow for a correction of some dipole field error. New designs for the end correction have been developed that may allow a single

setting for all gaps. Nevertheless, some correction is assured to be necessary in the end field tuning and there may be the need for gap-dependent adjustments. The tuning limit is set here to be equal to 5000 G cm, which corresponds to about 10% of the midplane flux in a single quarter period.

4.1.5 Axial Temperature Gradient

There is an additional limit on the structure associated with the variation in *K* caused by a temperature gradient axially along the insertion device. Since the allowable variation in *K* from this effect must be small compared to the variation calculated in Section 4.1.3, and the variation of *H* in Nd-Fe-B is about 0.12% *x* per degrees C, the axial temperature gradient limit is 2 degrees C for both the operation of the device in the machine and for the magnetic measurements.

4.1.6 Horizontal Magnetic Structure Requirements

The EW20.0 horizontal magnetic structure is an electromagnetic configuration. The poles are positioned between the vertical poles so that the horizontal field peaks are shifted 90 degrees with respect to the vertical field peaks. The horizontal field strength is changed by varying the current. Polarization is switched between left-handed and right-handed by switching the polarity of the current.

The deflection parameter, K_x, proportional to the contribution to the first integral of the horizontal field from a single pole, determines the vertical angle of the electron trajectory as it passes through the peak vertical field. Control of this quantity is directly linked to control of the degree of circular polarization. The production of an acceptable degree of circular polarization over the full operating energy range drives the allowed level of variation in integrated horizontal field from pole to pole. An experiment typically involves the subtraction of 2 data sets corresponding to the 2 polarities. The demands of this type of data analysis determine the required power supply stability. Table VI summarizes requirements.

Table VI. Horizontal magnetic structure requirements.

Pole to pole K_x, variation	< 2.0%
Variation between positive and negative polarities	< 0.01%
Short term stability in K_x (~ 1 hour)	< 0.01%
Long-term stability in K_x (~ 20 hours)	< 0.1%

A random variation in pole field integrals of 2% results in reduction of about 1% in the product of flux and degree of circular polarization for the low energy portion of the range (< 2000 eV). It results in about 2% reduction of the high energy range (> 2000 eV). The last 3 requirements are based upon simulations of magnetic circular dichroism (MCD) experiments. These requirements will incorporate into the power supply specifications. The required stability in K_x places requirements on temperature stability too, since temperature changes will result in dimensional changes in the magnetic structure and corresponding changes in K_x.

4.2 Magnetic Measurement Requirements

Several types of magnetic measurements will be made on the ALS insertion devices and their components. There are 2 major areas of magnetic measurements that are to be performed: 1) determining the magnetic characteristics of the Nd-Fe-B blocks, and 2) mapping the fields of the entire device. The requirements for each of these will be discussed in detail below.

4.2.1 Block Measurements

The principal dipole moment of each Nb-Fe-B block that will be used in the insertion device must be measured to an accuracy that will allow subsequent sorting into groups of 12 blocks to produce a standard deviation of

0.1%, or less, for the total moment on a single pole. The blocks proposed for the EW20.0 Elliptical Wiggler will have a volume of 90.0 cm^3 and a magnetic moment of about 9.6×10^{-5} Wb-m.

The rms-allowed variation when energizing the poles is 0.1%. If this is conservatively ascribed to, the rms deviation for the 12 blocks together, then the error in determining the quantity must be less—say half—or 0.05%. This leads to an allowable error in the measurement of the moment of each block given by:

$$\frac{\Delta M}{M} = \frac{1}{2}(0.10\%)\sqrt{12} = 0.17\%$$

Two factors can contribute to this error. The first is the measuring system itself, and the second is the temperature at which the block is measured. Moment measurements are considerably more accurate than 0.05% so they will contribute little to this error. However, the temperature coefficient of Nb-Fe-B, 0.12% per degree C, suggests it will be necessary to measure the temperature accurately and control it to better than 1 degree C and correct the measured moments for temperature.

4.2.2 Requirements For Measurements of the Full Insertion Devices

The requirements for the magnetic measurements of the full insertion device are based upon the requirements discussed in Section 3.0; the field quality must be adequate to produce radiation of the required quality and intensity and the insertion device must not have an adverse effect on the electron beam in the accelerator. These have been translated into allowable field errors that then determine the requirements for magnetic measurements.

EW20.0 differs from other ALS insertion devices in ways that require the development of new magnetic measurement instruments and techniques. Two significant differences are the presence of periodic horizontal fields in addition to vertical fields, and the horizontal field is time varying. The standard ALS insertion device measurement system was developed for fast and accurate Hall probe scans of devices that consist only of vertical magnetic structures. The presence of the EW20.0 horizontal magnetic structure precludes the installation of this scanning system. In addition, Hall probes are a poor choice for characterizing multidimensional fields because of the nonlinear planar Hall effect.

The magnet measurements must determine peak vertical and horizontal field values, the total axial field integrals and lateral variation in field integrals. Measurements must be made of local contribution to the horizontal field integral from individual poles and the mutual influence of the vertical and horizontal magnetic structures must be characterized. Measurements of the frequency dependence of the horizontal magnetic field must be made. AC measurements must be made in the presence of the vacuum chamber since this is where eddy current effects are expected to be most significant.

The existing Hall probe scanning system will be used to provide baseline measurements for the vertical and horizontal magnetic structures separately before they are integrated into the final configuration. A new dedicated magnetic measurement system will then be used for full characterization of the completed device. The new system will consist of a set of coils and fixtures, custom stages and transport systems. A long coil (at least 4 m long) will be used to measure total vertical and horizontal field integrals. One period and point coils will be used to measure local fields and field integral variations.

The requirements for magnetic measurements are summarized in Table VII.

TABLE VII. Magnetic Measurement Requirements for EW20.0.

Parameter	Value
Peak B_y	± 2.0 T
Peak B_x	± 0.1 T
Required measurement accuracy for B_y, B_x	± 1 G
$\int_{-\infty}^{\infty} B_y, dz, \int_{-\infty}^{\infty} B_x, dz$	100 G-cm
Required measurement accuracy	± 10 G-cm
$\int_{pole} B_x dz$	5125 G-cm
Required measurement accuracy	± 5 G-cm
Scan capability: z	4 m
x	± 2.5 cm
y	± 1.0 cm
Required scan position resolution: z	± 1 μm
x, y	± 25 μm

4.3 Vacuum System

The vacuum system specifications for the EW20.0 Elliptical Wiggler are driven by storage ring requirements.

4.3.1 Aperture Requirements

The clear aperture for the EW20.0 Elliptical Wiggler in the storage ring is similar to the injection straight; a 50 mm horizontal by 10 mm vertical rectangular opening.

4.3.2 Vacuum Requirement

The vacuum specification is based on cross-sections for scattering of the electron beam by the residual gas and ions in the vacuum chamber (the elastic scattering cross-section is 2/3 of the total and the inelastic scattering is the remaining 1/3) and leads to a 10^{-9} T vacuum requirement at 1.5 GeV—400 mA operation after 40 A h of operation.

4.3.3 Diagnostics

Beam position monitors are required at both upstream and downstream locations on the insertion device vacuum chamber for locating the electron beam.

5.0 Insertion Device Conceptual Design

The EW20.0 Elliptical Wiggler is a cross-field device; the vertical magnetic field is generated with a variable gap hybrid-permanent magnetic structure and the horizontal magnetic field comes from an iron core electromagnetic structure.[9]

This device features vertical and horizontal magnetic structures of 14 and 14.5 periods, respectively. The period length is 20.0 cm. The vertical structure is a hybrid permanent magnet design with tapered pole tips that produce a peak field of 2.0 T. The horizontal structure is an iron core electromagnetic design, shifted longitudinally 1/4 period, that is tucked between the upper and lower vertical magnetic structure sections. A maximum peak oscillating field of 0.095 T, at a frequency up to 1 Hz, will be achieved by excitation of the horizontal poles with a trapezoidal-current waveform.

The EW20.0 mechanical design is shown in FIGS. 4 and 5. The major subsystems identified are: the vertical magnetic structure, which includes the hybrid pole assemblies attached to the 3.4 m long backing beams; the horizontal magnetic structure, which includes a laminated electromagnet and associated support frame; the support and drive system, which includes the framework for supporting the magnetic structures and the mechanism for opening and closing the vertical magnetic structure gap; and the vacuum system, which includes a 3.6 m long stainless-steel vacuum chamber and its associated pumping system. The electrical design includes the control system for the vertical magnetic-structure gap drive, the vertical magnetic end structure power supplies and the horizontal magnetic-structure power supply.

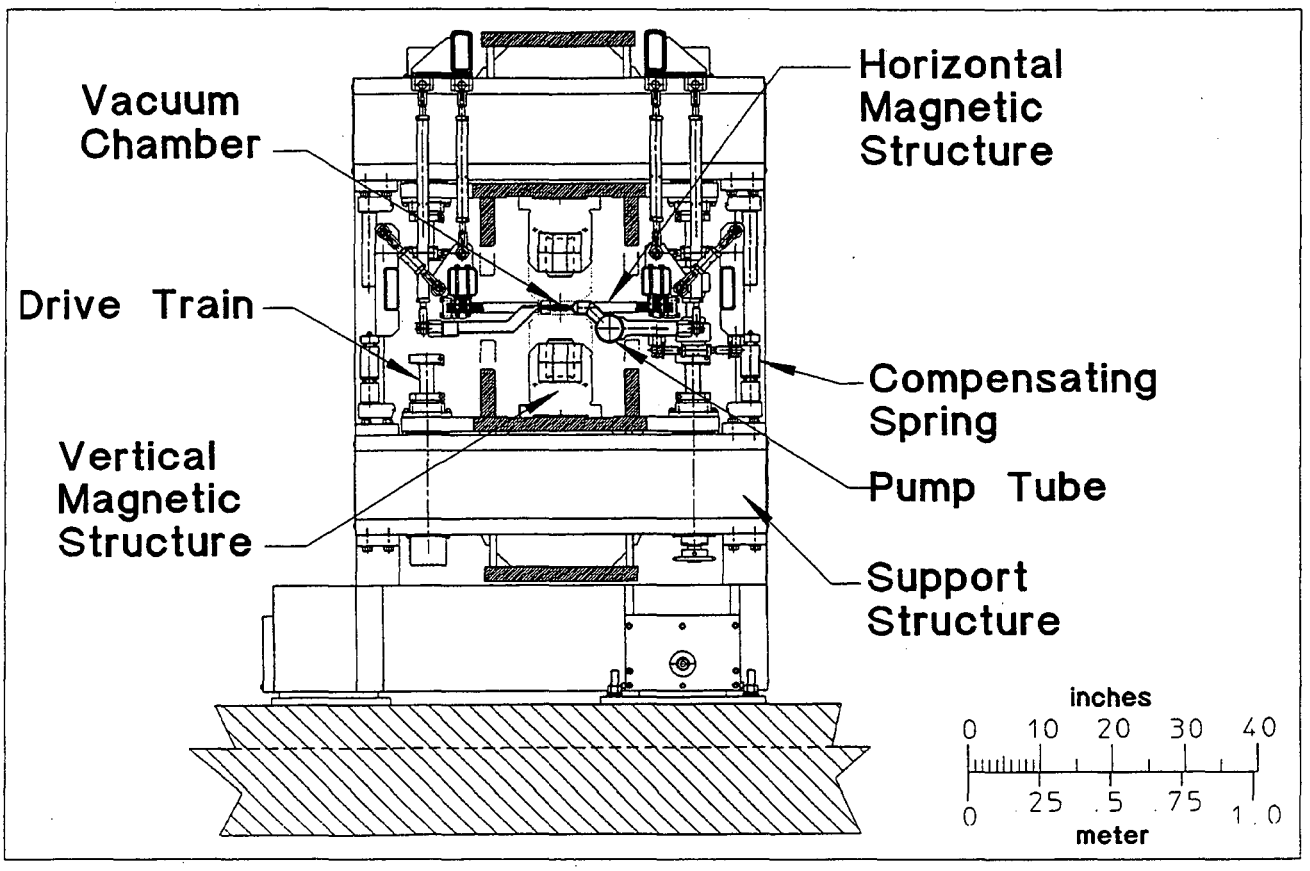

Fig. 4. EW20.0 Elliptical Wiggler—side view.

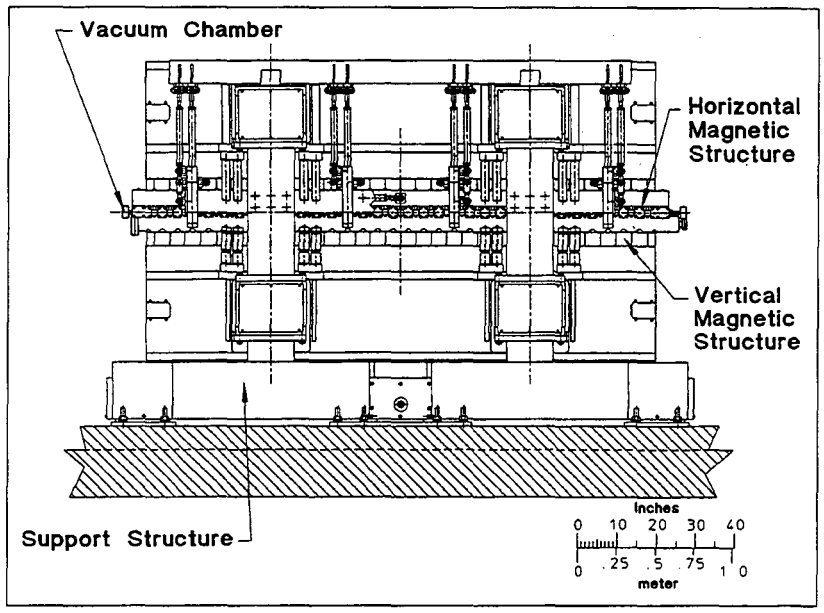

FIG. 5. EW20.0 Elliptical Wiggler—elevation view.

5.1 Design Philosophy

The approach taken for ALS insertion devices has been toward a generic design with the objective of reducing engineering and fabrication costs for easier maintainability.

In general, the following commonality by subsystem exists between devices:

Magnetic Structure

— Scaled wiggler magnetic configurations,
— Similar backing beams for the wigglers,
— Wiggler backing beams are shorter than the undulator backing beams.

Support/Drive System

— Identical support structures for the wigglers,
— Identical drive systems for all devices,
— Support structure shortened and widened for the wiggler.

Control System

— Identical control systems for all devices.

Vacuum System

— Similar vacuum chamber configurations for the wigglers,
— Wiggler vacuum chamber is similar to undulator's, but shorter; elliptical wiggler vacuum chamber is different.
— Identical pumping systems for the wiggler vacuum chamber,
— Similar pumping system for the wiggler; elliptical pumping system is different.

In general, the design, fabrication, testing, and installation of the EW20.0 Elliptical Wiggler vertical magnetic structure, support/drive system, and control system will be very similar to that of the ALS undulators and W16.0 Wiggler.[10]

5.2 Design Parameters

The following parameters in Table VIII have been established for the EW20.0 Elliptical Wiggler conceptual design.

TABLE VIII. EW20.0 insertion device engineering design parameters.

Vertical Magnetic Structure	
Peak Gap Magnetic Field Range	2.0 - 0.026 T
Vertical Structure Magnetic Gap Range	1.40 - 22.00 cm
Wiggler Period Length	20 cm
Number of Periods	14
Quarter Period Field Integral	4.41 X 10^4 G cm
Max. Horizontal Deflection Parameter (K_{yeff})	25.95
Max. Horizontal Opening Angle (@1.5 GeV)	+/- 8.82 mrad
Normalized Field Harmonics	
1st	1.0000
3rd	0.2712
5th	0.0794
7th	0.0186
Pole Width	8.0 to 10.0 cm
Pole Thickness	4.6 cm
Pole Height	13.4 cm
Nd-Fe-B Operating Point	0.519
Number of Nd-Fe-B Blocks Per Pole	12
Nd-Fe-B Block Size	2.7 x 5.0 x 6.7 cm^3
Vertical Magnetic Structure Length	343 cm
Maximum Pole Field	2.2 T
Entrance sequence	0, -1/4, +3/4, -1, +1 ...
End correction range (B_y)	5,000 G cm
End correction range (B_x)	None
Multiple trim magnet range	± 3,000 G cm
Horizontal Magnetic Structure	
Horizontal Magnetic Field	0.0947 T max.
Horizontal Structure Magnetic Gap	7.2 cm
Number of Periods	14.5
Horizontal Structure Length	3.53 m
Horizontal Half Period Field Integral	5,153 G cm max.
Max. Vertical Deflection Parameter (K_{xeff})	1.5
Max. Vertical Orbit Angles (@ 1.5 GeV)	+/- 0.510 mrad.
Pole Flux Density	1.96 T max.
Horizontal Field Frequency	1 Hz max.
Coil Design:	
Number of Full Field Coils	58
Number of 3/4 Field Coils	4
Number of 1/4 Field Coils	4
Number of Turns (Full Field Coil)	12
Current	500 A
Coil Conductor Length	80 inches (2 m)
Coil Resistance	3.51 mOhm
DC Power/Coil	879 W
DC Voltage/Coil	1.755 V
Coil Inductance	21.3 microHenry
Excitation Risetime	25 msec (min.)
AC Voltage/Coil	0.425 V
AC Power/Coil	213 W
Coil Time Constant	6 msec
Total DC Voltage	108.8 V

Total AC Voltage	26.4 V
Total Voltage	135.2 V
Total DC Power	53.1 kW
Total AC Power	12.9 kW
Total Power	66.0 kW
Coil Cooling:	
Maximum Flowrate/Coil (60 psi water)	0.38 gpm
Coil Temperature Rise	8.8 deg. C
Total Flowrate	25.1 gpm
Support/Drive System	
Backing beam length	3.46 m
Gap magnetic load (14 mm magnetic gap)	26,600 lbs.
Gap range	1.40–21.6 cm
Gap opening time	1 min.
Vacuum System	
Clear vertical aperture	10.0 mm
Maximum gap at pole windows	14.0 mm
Required pressure after 40 A-hr. of operation	10^{-9} Torr
Magnetic Structure/Vacuum Chamber Heating at 1 Hz	
Horizontal magnetic structure heating	6.6 W
Vertical magnetic structure Nd-Fe-B heating	1.0 W
Vertical magnetic structure pole heating	5.4 W
Vertical magnetic structure keeper heating	2.5 W
Vacuum chamber eddy current heating	1.0 W
Total heating	16.5 W

5.3 Vertical Magnetic Structure

The vertical magnetic structure is a hybrid permanent-magnet design which includes a periodic magnetic structure, end structures with correction coils, multiple trim magnets, and the 3.4 m long backing beams.

5.3.1 Vertical Periodic Structure Magnetic Design.

The periodic magnetic structure consists of Nd-Fe-B blocks and vanadium permendur poles.[11] The configuration is a rectangular pole with a tapered pole tip and Nd-Fe-B block array which is shown in FIG. 6. Generally, the principal objective of the design effort is to develop a magnetically well behaved structure which yields a high value of B_{max} and an adequate beam of radiation for midplane fields. The design approach utilizes 3-D hybrid theory and 2-D modeling with PANDIRA which is a sub-code of the POISSON Group of computer codes, and checking with the TOSCA code.[12, 13]

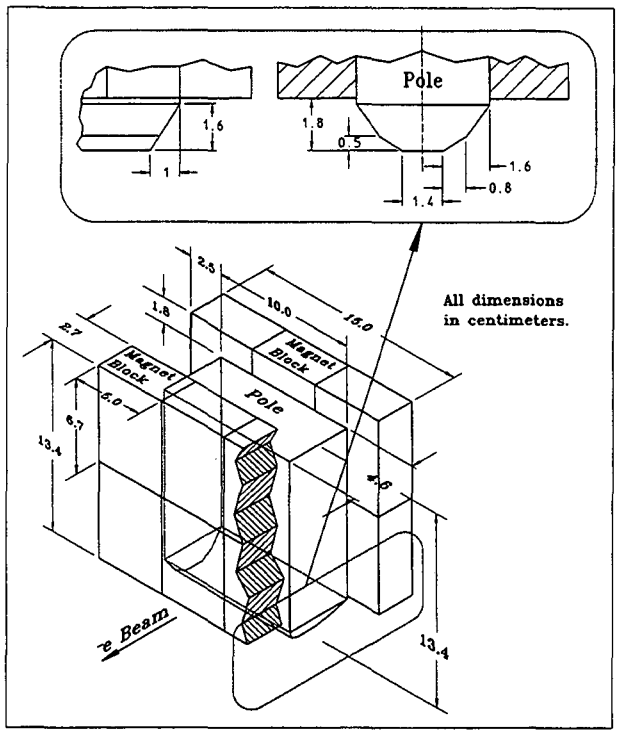

FIG. 6. Magnetic Structure — half-period configuration.

5.3.1.1 Calculation of Structure

PANDIRA allows convenient 2-D modeling of anisotropic materials. The Nd-Fe-B characteristics are defined by the remanent and coercive field intercepts of the linear B-H curve along with its easy axis orientation angle. The vanadium permendur is described by a nonlinear B-H curve which has been developed from measured data and is included in the input to PANDIRA.

2-D models are used to optimize the pole thickness and tip configuration, to provide detailed information about magnetic behavior and to provide flux information for the 3-D calculation. Vector potentials, which are the fundamental quantities calculated by PANDIRA, are used in detailed harmonic analyses and pole face investigations described below.

The optimum pole thickness is influenced by various parameters including pole tip geometry, saturation behavior of the pole material, operating point of the CSEM, and ratio of gap-to-period and spatial harmonics in the magnetic field. All of these geometrical and magnetic properties are defined and utilized in the 2-D PANDIRA models, which are used in the optimization of the pole thickness. For EW20.0, this optimization process yields a pole thickness of 4.6 cm.

The transverse width of the pole is determined by external considerations, such as constraint of dB_y/dx where x is the transverse direction (perpendicular to the beam). This pole tip dimension is 8.0 cm for the ALS undulators and is also used for EW20.0. The starting point of the Nd-Fe-B above the pole face is determined by space required for the horizontal field structure, as well as coercive-field effects in the permanent magnet material near the pole tip.

Application of the 3-D hybrid theory is necessary for the design procedure, since 2-D assumptions can yield configuration errors greater than 10%. The 3-D calculation separates the flux that enters and leaves the pole into what are called direct, or B_r fluxes, and indirect, or scalar, potential fluxes. The total direct flux for each pole is equal in magnitude to the total indirect flux associated with each pole. The direct fluxes come from the Nd-Fe-B and set the pole on a certain scalar potential. The indirect fluxes result from this scalar potential and are calculated for all surfaces and 2-D corners of the pole.

However, the hybrid 3-D calculation code normally used, HY3DCM2, assumes that the pole has infinite permeability, which is not valid in the case in the pole tip region of this high field device.[14] It is necessary to evaluate the computed geometry with a code which solves 3-D electromagnetic field problems taking saturation into account—TOSCA is used here. The geometry shown in FIG. 6 is the result of an iterative process where PANDIRA and HY3DCM2 were used in the design process, with TOSCA used in an evaluation mode.

The final dimensions of the structure come from balancing of the direct and indirect fluxes, where overhang dimensions and pole height are manipulated to achieve desired performance and minimal volume of Nd-Fe-B. The overhang contributes to the direct flux and causes an increase in the scalar potential of the pole.

In the case of EW20.0, with the Nd-Fe-B recessed from the pole tip to accommodate the horizontal field structure, pole shaping became necessary, as shown in FIG. 8, to prevent pole saturation. Calculations for EW20.0 require a pole height of 13.4 cm to achieve a 2.0 T peak field at the 14 mm gap.

5.3.1.2 Harmonic Content of Wiggler Fields

Harmonic Content is examined via Fourier analysis of the vector potentials calculated in 2-D by POISSON and PANDIRA. The periodic structure is assumed to be infinitely long and wide. The *y*-component of the fields in such a structure can be described by:

$$B_y(y,z) = B_1 \sum_{m=1}^{\infty} B_{2m=1} \cos[(2m+1)kz]\cosh\{(2m+1)ky\}$$

where $k = 2p/\lambda_u$, B_1 is the amplitude of the fundamental and $b_{2m+1} = B_{2m+1}/B_1$ is the normalized amplitude of the $2m+1$ field component.

The third harmonic (b_3) at the midplane for the pole design is 27.12% of the fundamental at the design gap of 1.4 cm, and decreases for larger gaps. Higher harmonics are smaller, $b_5 = 7.94\%$, $b_7 = 1.86\%$.

5.3.1.3 Block Sorting

To achieve uniform pole excitation and reduction of integrated error fields, which affect the electron beam trajectory, block sorting is required for the EW20.0 Elliptical Wiggler.

FIG. 7 shows a partial view of the lower magnetic structure of a typical ALS undulator. The orientation of the permanent magnet blocks is parallel to the *z*-axis (i.e., parallel to the direction of the electron beam). The vanadium permendur poles can be seen between the magnet block arrays. The electron trajectory is shown schematically (with exaggerated amplitude) centered above the upper-middle block of each magnet array. In the actual device, the structure is mirrored with opposite polarity above the electron beam trajectory.

5.3.1.4 Sorting for Uniform Pole Excitation

In order to establish uniform pole excitation, It is necessary that the average magnetic moment in the direction of magnetization, $\overline{M}_z$, for the magnet array associated with any pole, be the same as that of any other array. The first step of the sorting algorithm is to arrange blocks into groups of 6 using this $\overline{M}_z$ criterion.

For the EW20.0 Elliptical Wiggler, the moment values of the magnet block populations are determined by automated Helmholtz coil measurement. Values of M_x, M_y, and M_z are recorded to an electronic file. The data are then arranged in ascending values of a criterion called Γ_i calculated for each block, where:

$$\Gamma_1 = M_{xi}^2 + M_{yi}^2 \quad \text{for } i = 1 \text{ to } n \tag{1}$$

where n is the total number of blocks being sorted. The Γ criterion associates a combined minor component magnitude with each block. Blocks with lower Γ values are preferred for positioning close to the electron beam.

This ordered group is then subdivided into 6 subgroups with group 1 having the lowest Γ values, group 2 having the next lowest Γ values, and so on. Each of the 6 groups is assigned a position in the 6 block magnet arrays, as shown by the numbering scheme on the magnet blocks in FIG. 7. Thus, in this stage of the sorting process, any block from group 1 is constrained to a position immediately under, or above, the electron beam.

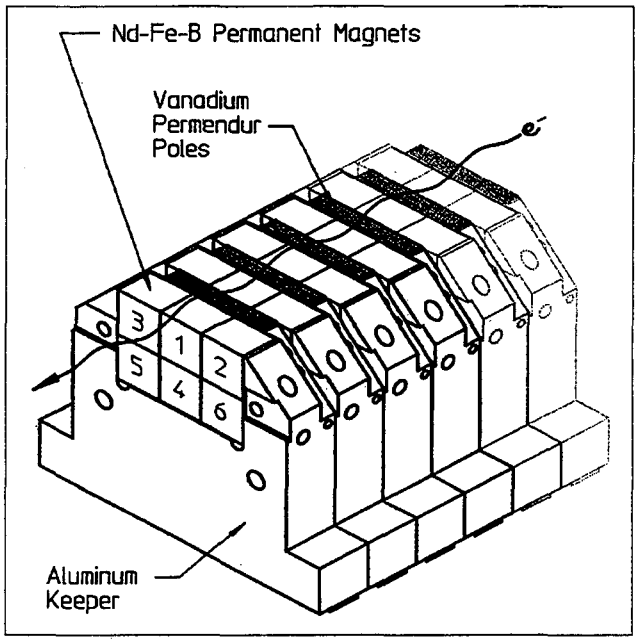

FIG. 7. Partial view of a lower half of an undulator's magnetic structure.

The next stage of the sorting process is to construct the 6 block magnet arrays. The objective here is to establish uniform averaged M_z values for the final 6 block arrays. This is done using a non-iterative ordering and pairing technique which is a feature of the NICOPOLIS sorting code groups. The steps of the process, as applied to a population of *n* blocks, are as follows:

1. The global average of M_z for the entire block population is calculated, and the deviation from that global average (dM_z) is calculated for each block.
2. The 6 groups, described above, are then monotonically ordered in ascending values of dM_z.
3. Groups 1, 2, and 3 are searched for the block having the greatest absolute value of dM_z.
4. The 2 groups which did not contain the block selected in Step 3 (above) are searched for the block having the greatest magnitude of dM_z of the opposite sign of that of the Step 3 block.
5. The blocks selected in Steps 3 and 4 (above) are paired and their dM_z values are averaged. They are also removed from the data set and stored along with their average dM_z value and group affiliations.
6. Steps 3–5 (above) are repeated *n*/3 times, which results in *n*/3 paired blocks and *n*/3 single blocks.
7. The *n*/3 pairs are monotonically ordered by their average dM_z values, and the single blocks are monotonically ordered by their dM_z values.
8. The ordered pairs and single blocks of Step 7, then, are paired by opposite extremes. The average *dMz* value of each of the resulting triplets is then calculated.
9. Steps 3–8 (above) are repeated for blocks in groups 4, 5, and 6.
10. The group 1-2-3 triplets, and group 4-5-6 triplets are separately ordered monotonically by their average dM_z values and paired by extremes to form the final 6-block arrays.

The above algorithm results in very rapid reduction in deviation from global average of M_z values for typical magnet block populations used in hybrid insertion devices.

When applied to a block population having an initial deviation of 4% for single blocks for a previous insertion device, the algorithm resulted in a final maximum deviation from global average at the 6-block array stage of less than 0.02%, which is below current, practical, and measurable levels.

5.3.1.5 Sorting for Reduced Integrated Field Errors

Extensions to the above described algorithm will be used to minimize the effects of minor component errors (M_x, M_y) on electron trajectories. A sufficient space for optimization remains after the sorting algorithm described in Section 5.3.1.4 is applied.

Parameters, such as block rotation and position shifts within 6-block arrays, as well and relocation of arrays in the magnetic structure will be used in conjunction with measured information about block-minor components to develop field-integral objective functions. Iterative optimization techniques, will be used to minimize these objective functions.

5.3.2 End Magnetic Structure Design

The EW20.0 end structures represent a departure from the designs for the ALS wigglers. The EW20.0 device uses a system of electromagnetic correction coils rather than permanent magnet rotors to fine tune the field distribution at the ends of the insertion device. The designed first-integral field-tuning capacity of these correction coils is 5000 G cm at each end of the device. This is more than 10% of the integrated midplane flux from a quarter period of the interior periodic field of the device.

The entrance scheme for the device consists of a nominal, normalized scalar potential distribution of 0, 1/4, -3/4, 1, -1..., etc. This uncorrected scalar potential distribution is determined by diminishing quantities of fixed permanent magnet material at the ends of the magnetic structure. The device has an even number of poles, which implies an exit scheme with the same scalar potential magnitudes, but with the opposite signs.

FIG. 8 is a longitudinal cross section of the end of the magnetic structure installed on the backing beam. The pole indexing convention is given in this figure with the first, or field clamp, pole designated as pole "0," the second as pole "1," and so on. The correction coil can be seen around pole 1.

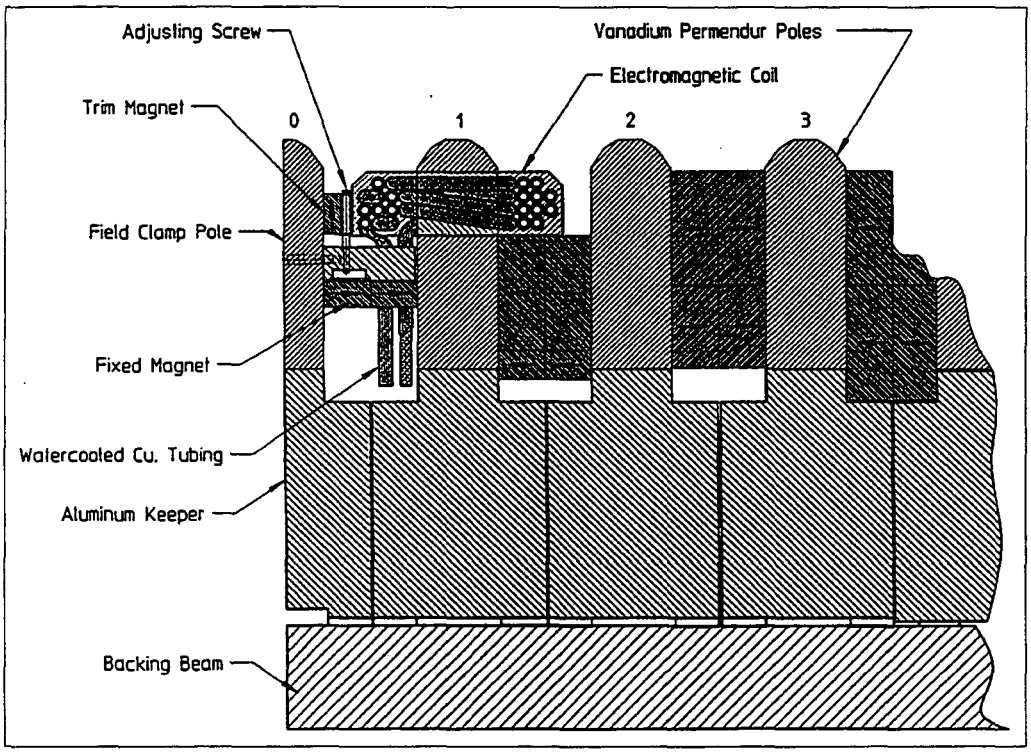

FIG. 8. U10.0 Wiggler end magnetic structure.

The volume of the fixed material between poles 0–3 is selected via 3-D numerical modeling to produce the 0, 1/4, -3/4 normalized scalar potential distribution mentioned previously. From pole 3 on, the volume of the permanent magnet material is uniform until the opposite end of the device is reached. The opposite end of the magnetic structure has the same permanent magnet volume distribution but with opposite order and polarity.

5.3.3 Multiple Trim Magnets

Multiple trim magnets will be designed into the end structures to reduce the higher order fields to meet the accelerator requirements in integrated magnetic field errors.[15]

Application of the multiple trim magnets on the U5.0 and U8.0 wigglers has demonstrated better than an order of magnitude reduction of both the normal and skew integrated magnetic field errors.

A flux plot of a trim magnet in an insertion device structure is shown in FIG. 9. The field produced at the midplane by the trim magnet may be varied by adjusting the size, position, and orientation of the magnet. To correct integrated magnetic field errors in the device aperture, a transverse array of these trim magnets is used.

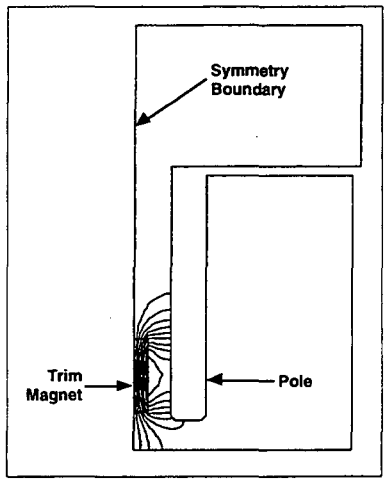

FIG. 9 Flux plot of a single trim magnet in an insertion device.

5.3.4 Vertical Periodic Magnetic Structure Mechanical Design

The basic building block of the periodic magnetic structure is the half-period pole assembly, which consists of an aluminum keeper, a vanadium permendur pole, and 12 Nd-Fe-B blocks, and is shown in FIG. 10.

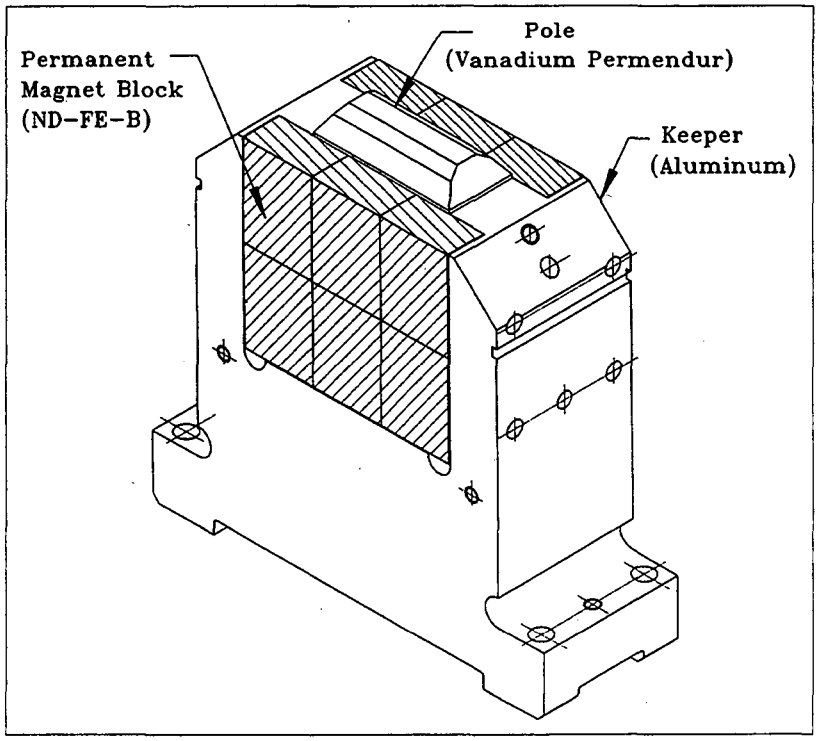

FIG. 10. EW20.0 half period pole assembly

The vanadium permendur poles will be machined, heat treated, and then finish ground. Each pole will be pinned to its keeper with 4 stainless steel pins, and secured with 4 stainless steel screws. All the pole and keeper assemblies will have a final trimming grind on the back of the keeper so that the overall height of all these assemblies will be within 25 μm.

For the EW20.0 Elliptical Wiggler, 708 full-size Nd-Fe-B blocks, and 60 smaller Nd-Fe-B blocks are required. To account for block breakage, blocks that do not meet specifications, that are incorrectly assembled, and damaged pole assemblies, will require the purchase of about 6% extra blocks for an 816 block total.

The Nd-Fe-B permanent magnet blocks for EW20.0 are to be ordered per LBL Specification, M802.[16] Key sections in Specification M802 include:

Magnetic Properties:

2.1 A nominal coercive force of 10.6 kOe after thermal stabilization ~ at 25° C.

2.2 A nominal intrinsic induction, that is linear within 2.5% to at least 120% of the nominal coercive force at 50° C after thermal stabilization.

2.4 Blocks thermally stabilized at 60° C for 3 hours.

2.5 The direction of magnetization, easy-axis, to be within ± 3°.

Mechanical Properties:

3.1 Block dimensions are 26.87 mm thickness [direction of magnetization] x 50.00 mm width x 67.00 mm length. Thickness tolerance is ± 0.070 mm. Width and length tolerances are ± 0.25 mm.

Coating Information:

4.1 Blocks to be suitably coated with a metallic coating, thickness at least 0.010 mm and not to exceed 0.030 mm, to prevent corrosion in a 25° C, 75% relative humidity environment.

Packaging:

6.1 Blocks are to be shipped in foam cubes, 10 cm on a side, to make subsequent handling at LBL easier.

The Nd-Fe-B blocks will be inserted into the pole assembly using a block holder and then held in place with a bonding fixture. The adhesive will be cured at room temperature.

Half-period pole assemblies will be mounted directly onto the backing beams. To achieve the target 25 μm pole height variation on the magnetic structure will require shimming between the half-period pole assemblies and the backing beams. A cross section of the EW20.0 Elliptical Wiggler is shown in FIG. 11.

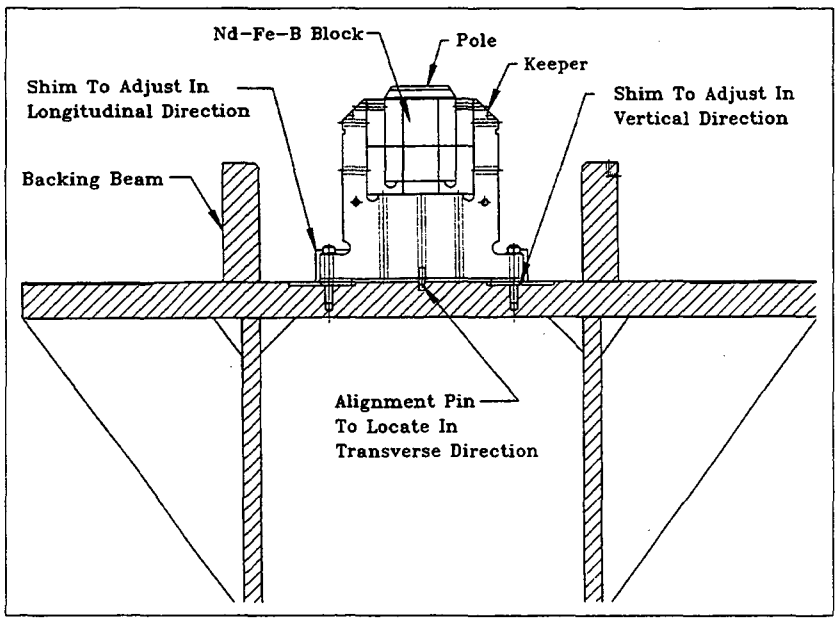

FIG. 11. U5.0 Wiggler assembly section.

5.3.5 Vertical End Structure Mechanical Design

A 14-turn mandrel wound coil with water cooled, continuous, hollow copper conductor is shown in FIG. 8. The coil is to be wound, then potted in epoxy after sleeving with fiberglass insulation. The maximum anticipated total current (NI) per coil is 1000 amps, which is derived from 3-D field modeling of the complete, nonlinear, end magnetic structure. The coil will be mated to a bipolar power supply with a stability specification of (±) 0.01%.

5.3.6 Multiple Trim Magnets Design

The correction of the higher-order integrated magnetic field errors is done with the multiple trim magnets. The EW20.0 multiple trim magnet configuration will be similar to that developed for the U5.0 undulator, which is shown in FIG. 12. To change the field integrals, the trim magnets can be adjusted vertically up or down, or they can be replaced with different size trim magnets.

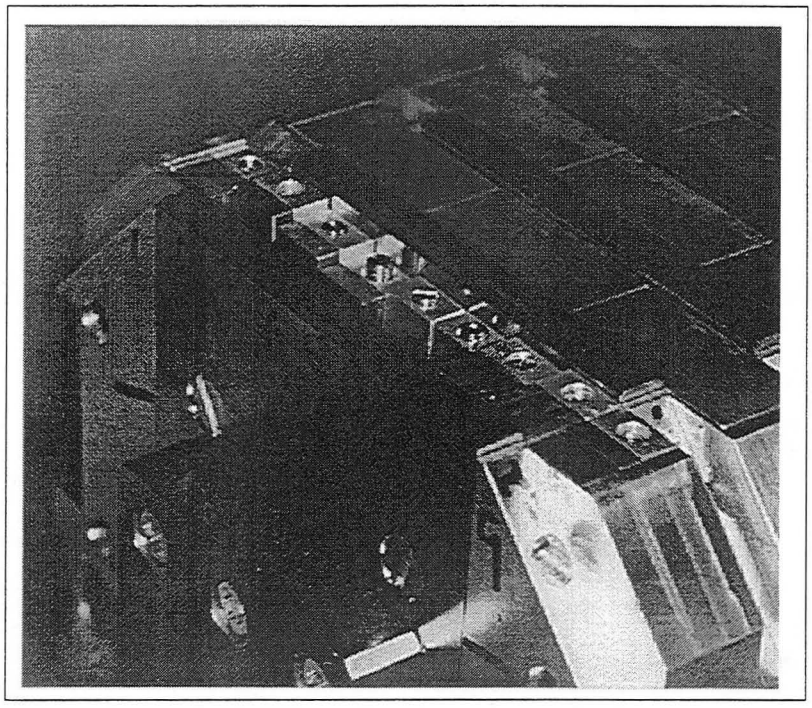

Fig. 12. U5.0 Undulator multiple Trim Magnet Array.

5.3.7 Field Error Corrections Design

Capability is provided for correcting local steering errors by either adding permanent magnet, or iron shims, symmetrically to pole pairs to produce local steering fields. Two cylindrical holes are provided in each keeper assembly, close to the pole face, which extend to the pole where permanent magnet material, or iron, can be positioned as a backup to shimming. Tuning coils can be designed into the magnetic structure in the event that difficulty is encountered in achieving the required field performance.

5.3.8 Backing Beam Mechanical Design

The backing beam, shown in FIG. 13, will be a skirted-box section design with a very rigid moment of inertia to length ratio resulting in minimum deflection due to the magnetic load on the backing beam. The backing beam will be a welded steel construction. To minimize material creep, the welded backing beam will be rough ma-

chined, stress relieved, and final machined. The support points for the backing beam will be located to achieve small deflections.

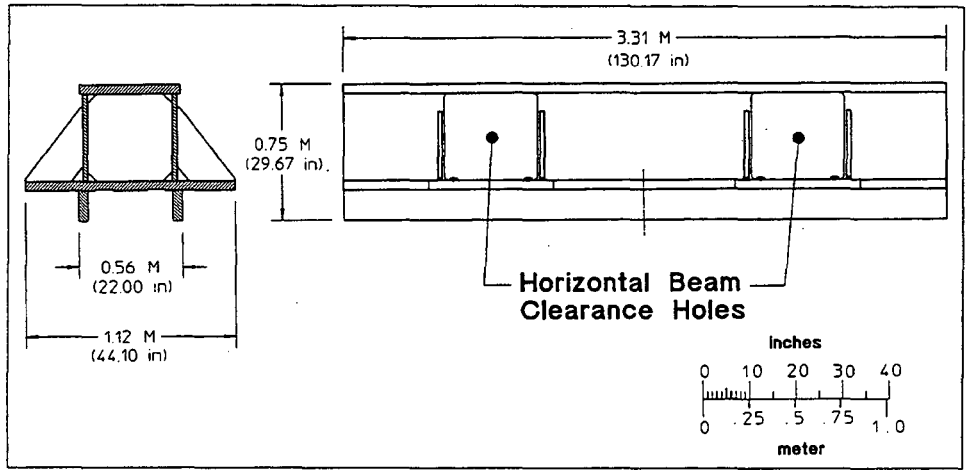

FIG. 13. Backing beam configuration.

Backing beam deflection calculations, carried out for the EW20.0 Elliptical Wiggler magnetic loading, give the follow results:[17]

Deflection of beam without cutouts	1.0 μm
Additional deflection due to cutouts	0.5 μm
Additional deflection due to support location errors	0.1 μm
Total deflection due to magnetic loading	1.6 μm

Deflections of the beams due to their own weight—provided they are equal—do not affect the gap variation. Of more concern are deflections due to a vertical temperature gradient in a backing beam. These deflections are:

- 3.4 μm/0.1 degree C at the center of the beam.
- 7.8 μm/0.1 degree C at either end of the beam.

To minimize deflections due to vertical thermal gradients will require good vertical circulation of the air at the insertion devices. Fortunately, the thermal time constant of the backing beams is long—24 hours—compared to a typical photon run of 8 hours, and can be increased to 40 hours with the addition of a 1/2 inch layer of Ensolite foam.

5.3.9 Magnetic Structure Alignment

Magnetic structure alignment is carried out using techniques developed during the assembly of the U5.0 and U8.0 Undulators.[18]

The current mechanical arrangement, as shown in FIG. 14, consists of a direct interface of the pole assemblies to the backing beam. In the previous ALS undulator magnetic structures, pole assemblies were placed on separate pole mounts, and formed independent magnetic structure modules which were then attached to the backing beams.

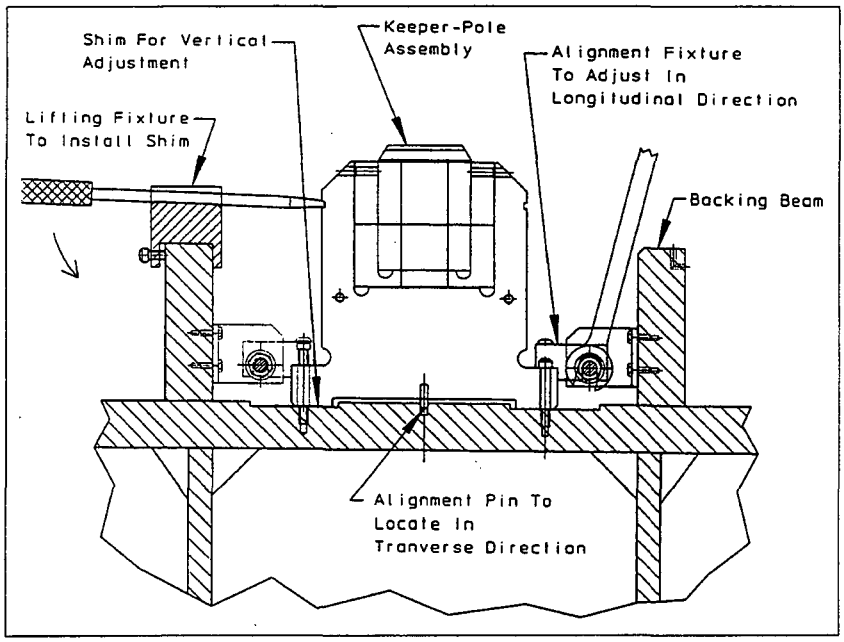

FIG. 14. EW20.0 vertical magnetic structure alignment and adjusting features.

A locating key at the bottom center of the pole assembly in FIG. 14 provides lateral or X-direction restraint of the pole assemblies in the backing beam. The magnetic structure has the largest position tolerance budget (~ 500 microns) in the X direction. This tolerance is large enough to be met by location specification of the keyway in the backing beam and the mating dowel pin shown in the bottom of the pole assembly.

Laser interferometer techniques will be used to perform the longitudinal and vertical precision alignment of the pole assemblies in the backing beam. Pole assemblies will be shimmed to meet the vertical tolerance and removable longitudinal adjustors, shown in FIG. 15, will be used for horizontal positioning.

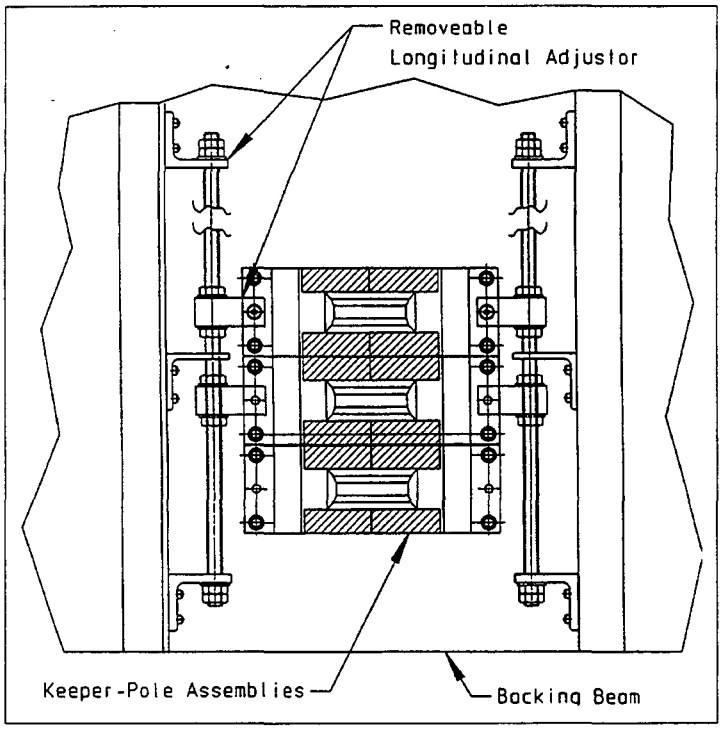

Fig. 15. EW20.0 vertical magnetic structure horizontal adjustment hardware.

5.4 Horizontal Magnetic Structure

The horizontal structure, an electromagnetic configuration, includes a periodic structure, end structures, auxiliary trim coils and its associated support frame, as shown in FIG. 4 and 5.

5.4.1 Horizontal Magnetic Structure Magnetic Design

The horizontal magnetic structure has the same period length as the vertical magnetic structure but is longitudinally phase shifted 1/4 period relative to the vertical magnetic structure. To avoid linear polarization contamination of the circularly polarized photon beam, the magnetic field distribution includes 14.5 periods. Thus, at both wiggler ends, the horizontal structure extends 1/4 period past the vertical structure.

To achieve the 0.095 T peak field, the poles and coils of the horizontal magnetic field structure are tucked between the upper and lower vertical magnetic field structures as shown in FIG. 16. The pole region geometry of the horizontal magnetic structure is shown in FIG. 17. A 1/4 period flux plot (cylindrical geometry used) of the selected horizontal magnetic structure geometry, generated with the POISSON code, with the vertical field pole is shown in FIG. 18.

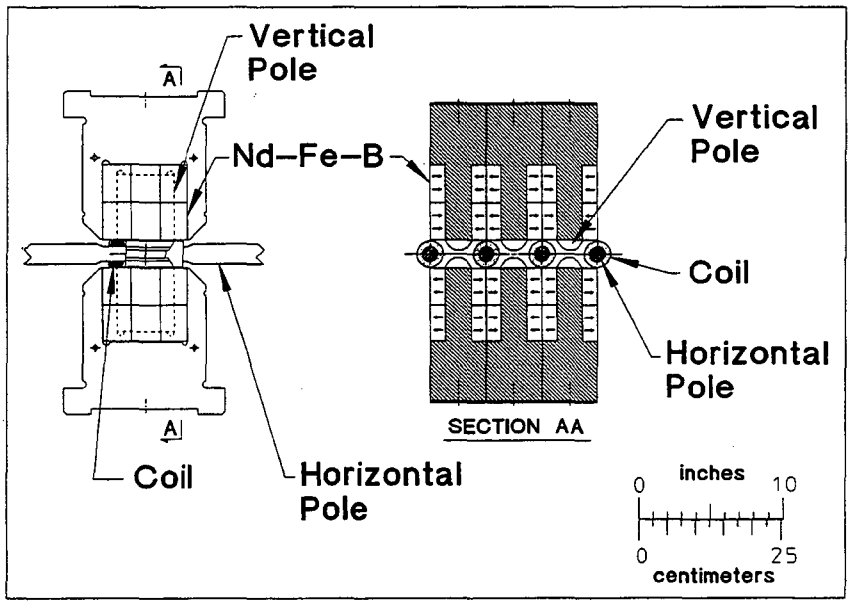

FIG. 16. EW20.0 vertical and horizontal magnetic structure.

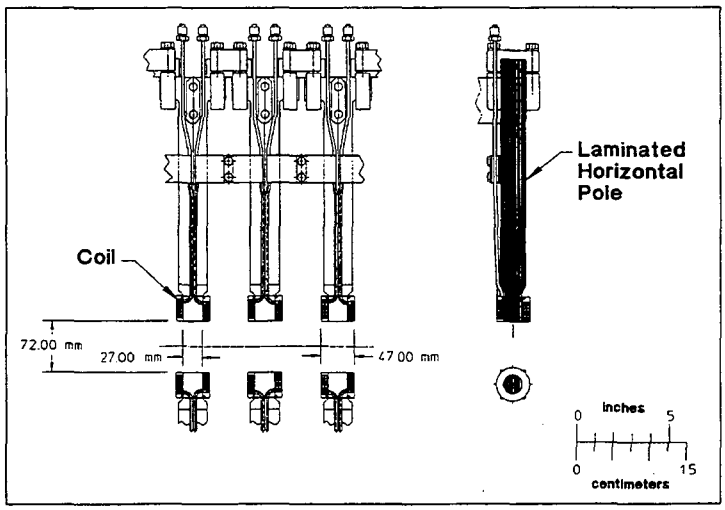

FIG. 17. Horizontal magnetic structure pole-coil construction.

Spectral calculations indicate that a 2.0 % time invariant half-period field integral error is tolerable for the horizontal structure. Magnetic structure mechanical tolerances can be calculated based on magnetic field sensitivities to dimensional changes of the magnetic structure to establish a tolerance budget. Magnetic field sensitivities, due to dimensional changes of the horizontal magnetic structure, are calculated using the model shown in FIG. 18, and given in Table IX.

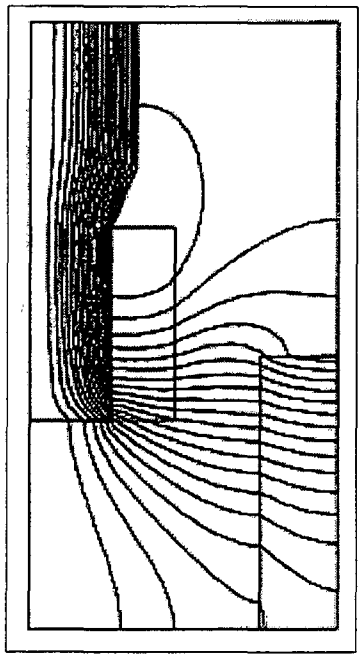

FIG. 18. Horizontal magnetic structure flux plot.

Table IX. Peak magnetic field sensitivities due to dimensional changes in the horizontal magnetic structure.

Dimensional Change	Sensitivity Coefficient (% Field Integral change/mm)
Pole Half Gap	4.72
Pole Radius	8.70
Transverse Coil Position	0.90

Based on the above sensitivity coefficients, the following mechanical tolerances tabulated in Table X for the horizontal structure are suggested to meet the 2.0% field integral error allowance.

Table X. Horizontal Magnetic Structure Pole Region Tolerances

Dimension	Tolerance (mm)	Field Integral Error (%)
Pole Half Gap	0.25	1.18
Pole Radius	0.125	1.09
Transverse Coil Position	1.00	0.90
Total		1.84

The ends of the magnetic structure have the same normalized potential structure as that for the vertical field, 0 , -1/4, +3/4, -1, +1, ..., etc. To achieve the appropriate pole potentials, the number of turns are reduced in the excitation coils proportional to the desired pole potentials. Field corrections can be accomplished by either mechanically adjusting the magnetic structure, or by exciting trim windings.

5.4.2 Horizontal Magnetic Structure Mechanical Design

The basic horizontal magnetic structure mechanical design is shown in FIG. 17. The electromagnetic coils are of conventional design. The coil conductor is 4 mm square by 2.5 mm inner diameter copper conductor that is turn-to-turn insulated with 0.007 inch thick fiberglass sleeving. Ground insulation is with 4 layers of 0.007 inch thick fiberglass tape half-lapped. Last, the insulated coil is vacuum impregnated with epoxy. Coil connections, interlocks, safety and testing follow ALS practice.[19]

The horizontal structure cores are epoxy laminated from 0.64 mm thick, M-36 electrical steel punchings to provide the configuration shown. These cores are clamped to square steel tubes with aluminum spaces and shimmed to meet the required mechanical tolerances. The cores are insulated from one another with Kapton film.

The horizontal magnetic structure, two sections, are mounted off the wiggler support structure with struts, which position and allow adjustment of the horizontal structure as shown in FIG. 4.

5.4.3 Horizontal Magnetic Structure Power Supply

Coil excitation of the series string of horizontal coils is done with a bipolar-regulated power supply that will provide a trapezoidal wave form for frequencies from DC up to 1 Hz, and capable of full four-quadrant operation. The supply will have sufficient voltage capability to drive the coils to produce a trapezoidal wave shape of current that is bipolar with a maximum value of +/- 500 A. The rate of change of current between positive and negative values will be 20,000 A/sec. This translates to a 50 msec transition between the maximum positive and negative currents. Therefore, if the system is operating at a 1 Hz rate, the transition time will be 10% of the period (some additional time will have to be allowed for the current to settle within the required tolerance). With a sum inductance of 1.3 mH for the coils, the required forcing voltage is 26 V, and the IR voltage is approximately 110 V, so the overall voltage rating will be around 160 V.

It is necessary that the current at flattop (after settling) be repeatable to within ± 0.01% during data-taking runs of approximately one hour. The settability of this current is ± 0.1%. The system will run under closed-loop current control, with the current monitored by a wideband zero-flux transductor. There will be means for local and remote generation of the desired reference wave shape. The repetition rate of the trapezoidal, bipolar wave shape will be variable from 0.1–10 Hz. Running the system as a bipolar DC current- controlled supply of the same rating will also be possible.

The 4-quadrant operation means that a reverse voltage can be applied when the current is at flattop value, forcing the current towards zero. This forcing voltage will continue to be applied as the current increases in the opposite polarity until the current reaches the desired value. During these transitions, the power is reversed from the load to the power system during the time the current and voltage are of opposite polarities. In the proposed design, the power reversal will store energy in the DC power supply capacitor bank until It flows back to the magnet in the next cycle.

Initially, the power supply must be interlocked so that the minimum reversal time of the current is equal—or greater than—50 msec to prevent permanent damage to the vacuum chamber.

5.5 ID Magnetic Measurement Facility

Two general types of measurements are needed for insertion devices: I) block measurements for determining the magnetic characteristics of the Nd-Fe-B blocks, and 2) insertion device measurements for mapping the fields of the entire device.

Block measurements include mechanical measurements and Helmholtz coil measurements to determine the major and minor magnetic moments.[20] The insertion device will be measured with a combination of existing equipment and new specialized equipment developed specifically for EW20.0 measurements. The following measurements are planned:

1. Field mapping of the vertical and horizontal magnetic structures before integration into the completed insertion device. These measurements will use the existing Hall probe scanning system.[21]
2. Vertical and horizontal field mapping of the integrated device. These measurements will use a point coil and a new coil transport system, described below.
3. One period length coil (null coil) scans of horizontal and vertical fields. These measurements will also the new coil transport system.
4. Long coil measurements to determine full-device vertical and horizontal field integrals. This will use a modified existing 5.5 m coil.
5. Measurements at the end of the device to characterize and adjust end trim coil response. These measurements will use an existing Halbach end coil.[22]
6. Measurements to assess eddy current effects. These measurements will be made inside a prototype vacuum chamber section while modulating the horizontal field. They will use the point coil and 1-period coil with the transport system and the long coil.

The following features of the EW20.0 design motivate the development of a specialized Measurement system:

1. The horizontal magnetic structure interferes with the installation of the standard Hall probe scanning stage.
2. The horizontal magnetic field will be time modulated, so AC measurements must be made.
3. The nonlinear planar Hall effect make Hall probe measurements problematic in the presence of strong vertical and horizontal fields.

The new Measurement system will include a set of small coils and a computer controlled transport system to scan coils along the z-axis of the device. The transport system will consist of a carriage for holding small coils, a cable/stepper, motor/pulley arrangement for moving the carriage, and a guide rail to maintain the *x* and *y* position as the carriage translates in the *z* direction. The carriage, cable, and guide rail must be made of nonmagnetic and nonconductive material. The system is shown schematically in FIG. 19.

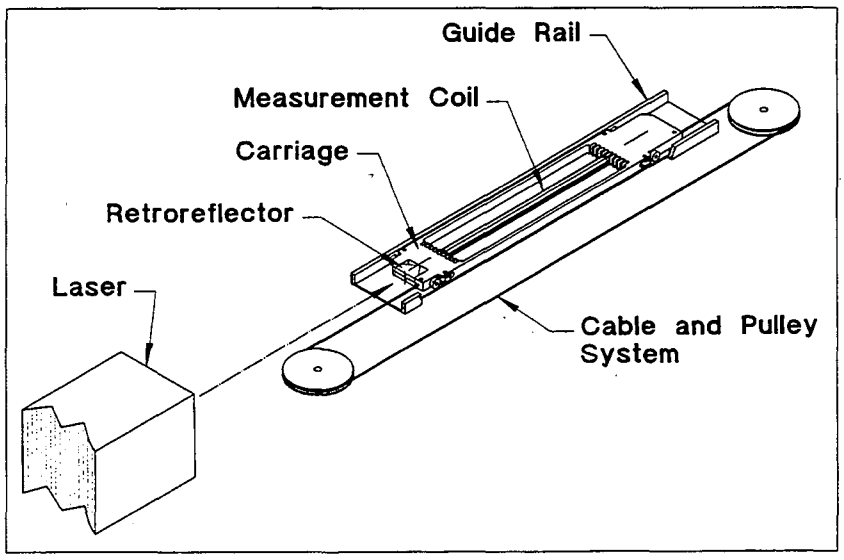

FIG. 19. DC/AC magnetic Measurement shuttle.

5.6 Support/Drive System

The support/drive system includes the support structure that provides the framework for holding the magnetic structure and the drive system, which will open and close the vertical field structure gap. The EW20.0 Elliptical

Wiggler Support/Drive System is a shorter and wider version of the generic ALS Support/Drive System, and thus, similar to the U5.0, U8.0, and U10.0 Undulator Systems. A description of that system follows.

5.6.1 Support Structure Design

The support structure is designed to support a maximum magnetic load of 84,000 lbs, the loading due to a 1.85 T field, 10 cm wide pole in a 5 m long wiggler, which is adequate for the EW20.0 Elliptical Wiggler. The support structure design developed is compatible with the storage ring tunnel and the adjacent beamlines. It can accommodate the vacuum system and has an alignment method and a floor support system.

The support structure design of the EW20.0 Elliptical Wiggler (W16.0 Wiggler support structure is identical) is shown in FIGS. 4, 5, 20, 21, and 22. Building from the floor, the support structure consists of a base onto which 2 horizontal beams are mounted, then 4 vertical posts are mounted, and finally, the 2 remaining horizontal beams. The 4 horizontal beams carry the backing beams of the magnetic structure. These horizontal beams are inserted through the webbing of the backing beams to minimize the overall height of the support structure to less than 8 feet. (As previously explained in Section 5.3.8, these cutouts in the webbing of the backing beams only cause small additional beam deflection.)

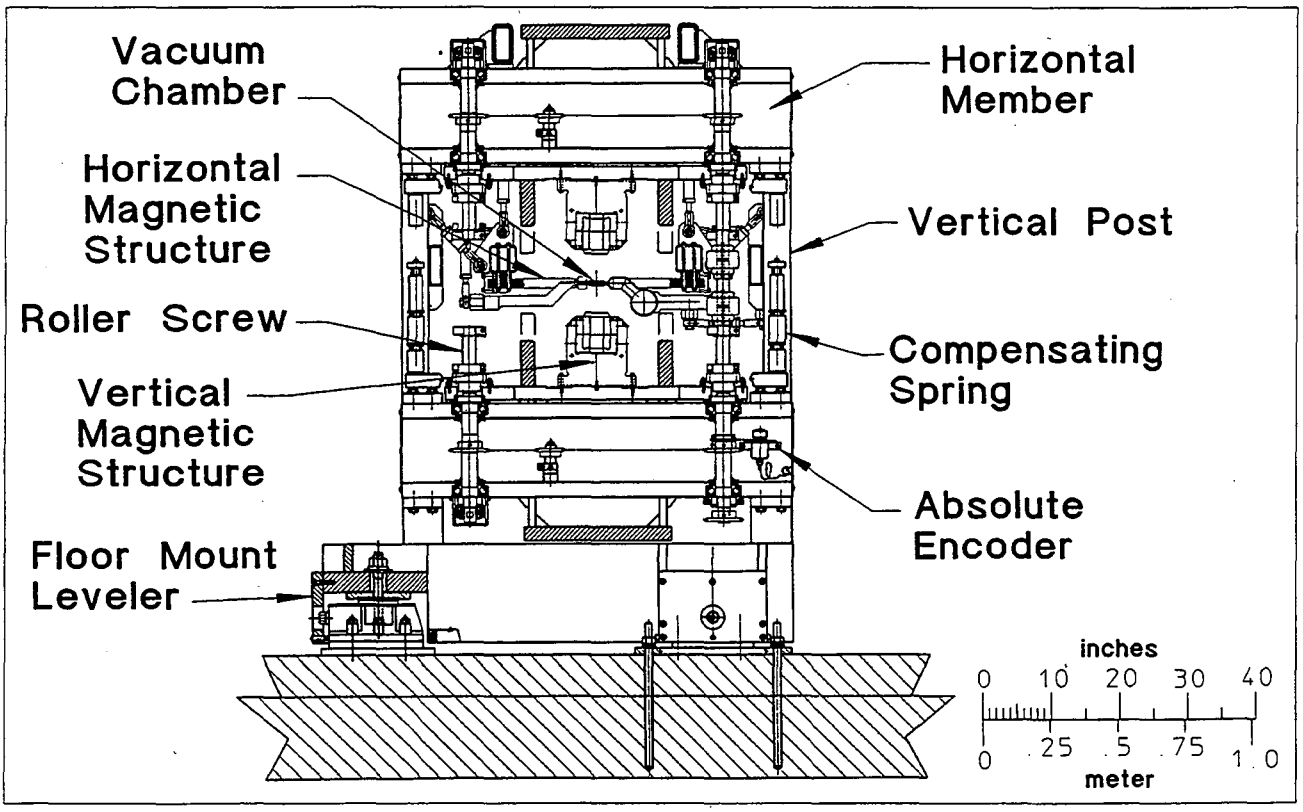

FIG. 20. Elliptical Wiggler end view.

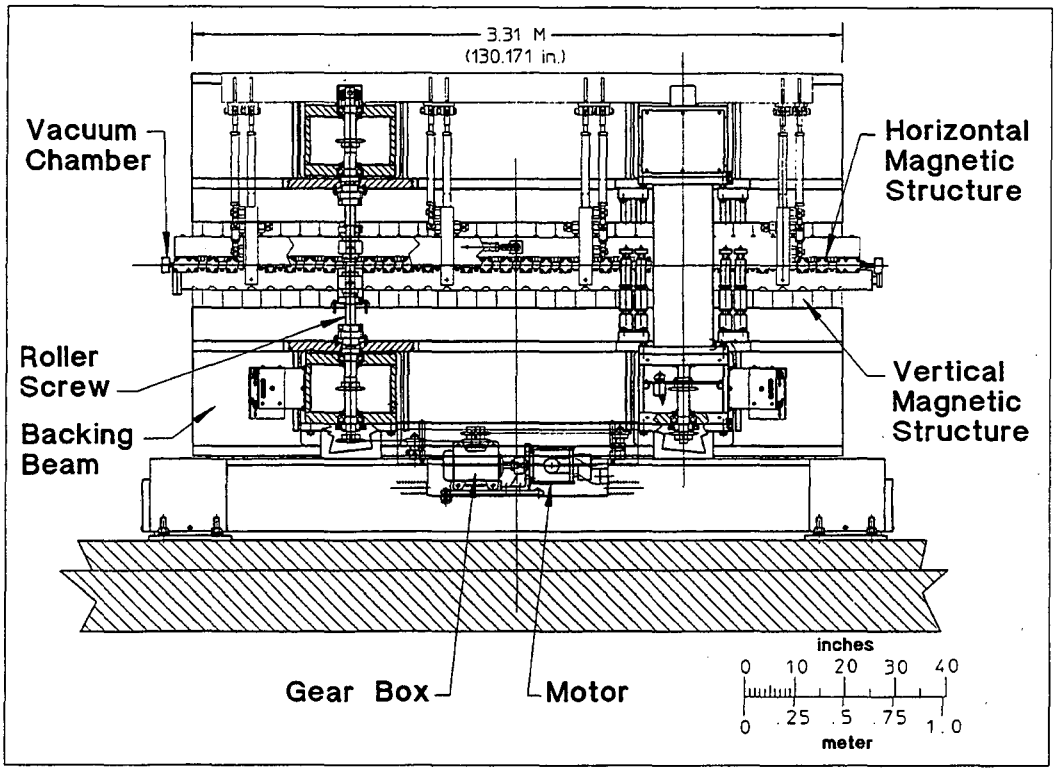

FIG. 21. Elliptical Wiggler — elevation view.

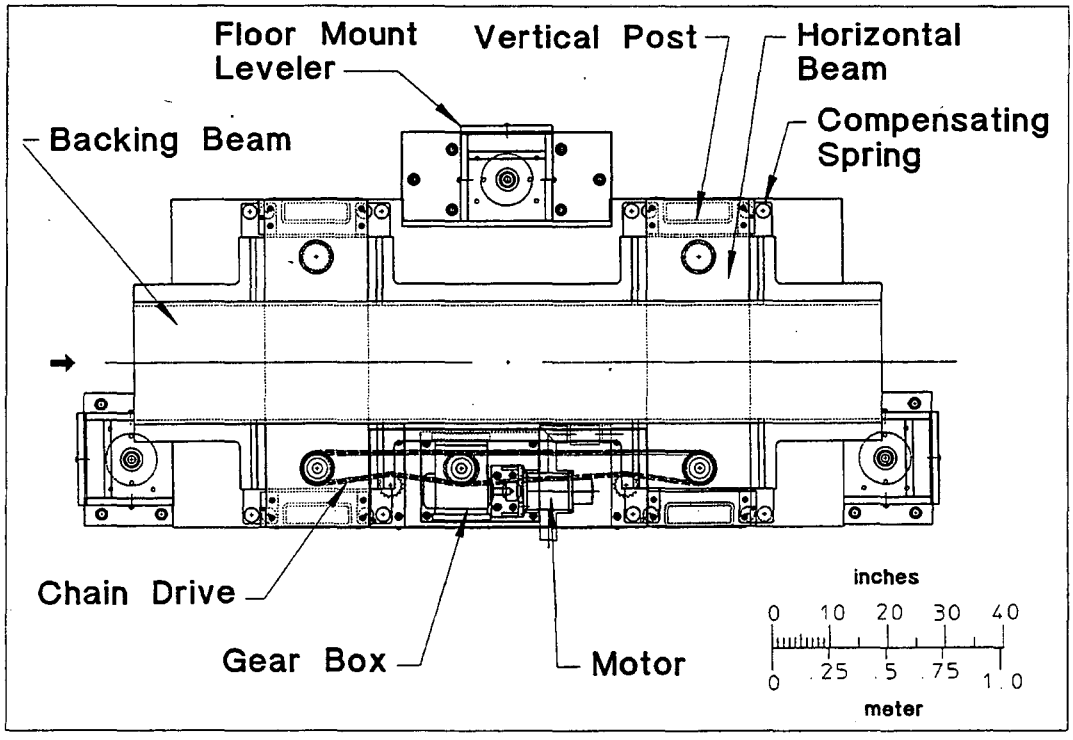

FIG. 22. Elliptical wiggler — plan view.

The base is a welded assembly containing 3 *y*-axis leveling mounts for a kinematic support system. The *x* and *z* axis adjustments are also provided at each leveling mount. This arrangement provides a limited but satisfactory range of adjustments for alignment in all 6 degrees of freedom needed for installation and alignment.[23] The

four vertical posts and 4 horizontal beams are bolted together and to the support frame. This modular arrangement allows for ease of fabrication, installation, calibration and servicing. All subassemblies are stress-relieved before final machining to minimize material creep.

During assembly, survey fiducials are placed on the 4 vertical posts, and various other surfaces, to facilitate installation alignment of the wiggler in the storage ring. Either optical tooling survey alignment, or ALS coordinated surveying system, will be used for the final alignment. Periodic leveling to accommodate ground settling will use the same *y*-axis leveling mounts.

A magnetic load compensating spring system will be provided to buck the gap dependent magnetic load similar to that used on the U8.0 Undulator.[24] The system will utilize 16 assemblies of different compression springs set in-line with appropriate stops to match the magnetic load to within 20% of the a 26,500 pound magnet load at a 14 mm gap.

The compensating spring system provides the following advantages:

1. Reduced system friction, which gives better positional response from the drive system.
2. No motor load holding torque required at any magnet gap, which gives stationary stability when the null position is reached. Motor current can be turned off or reduced to minimize motor heat-up.
3. Elimination of "lifting" when the magnetic load exceeds the gravitational beam weight of the lower backing beam.
4. Reduced structure compression, which gives better gap reproducibility.

5.6.2 Mechanical Drive System Design

The generic drive system design capabilities include opening the magnetic gap with an 84,000 pounds magnetic load; a step resolution < 1.02 μm (based on 1/10 of the 5th harmonic of a U3.65 undulator); a velocity > 2.31 mm/sec (based on a scan rate of 1 bandwidth/sec for an 11 cm period device). Interfacing with the control electronics allows for both local and remote control. The magnetic gap range will be 14–220 mm.

Various aspects of the drive system are shown in FIGS. 20, 21, 22, 23, and 24. The backing beams are supported by the Transrol roller screws. These roller screws are in turn, all connected together with a system of roller chains, sprocket wheels, and spring-loaded idler sprocket wheels. A gearbox and a stepper motor drive the system. An absolute rotary encoder is coupled to a Transrol roller screw shaft to read the absolute position of the magnet gap.

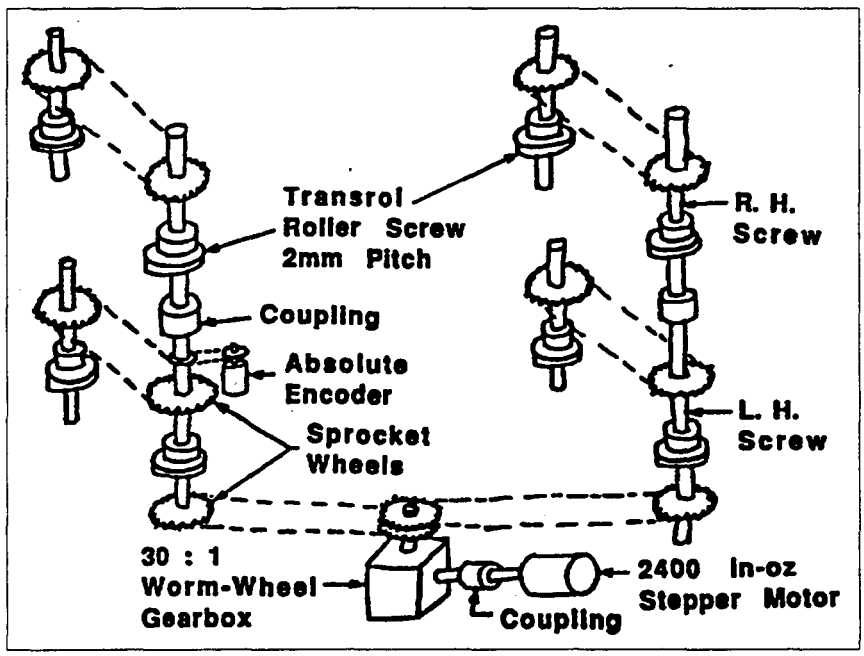

FIG. 23. Elliptical Wiggler drive system schematic.

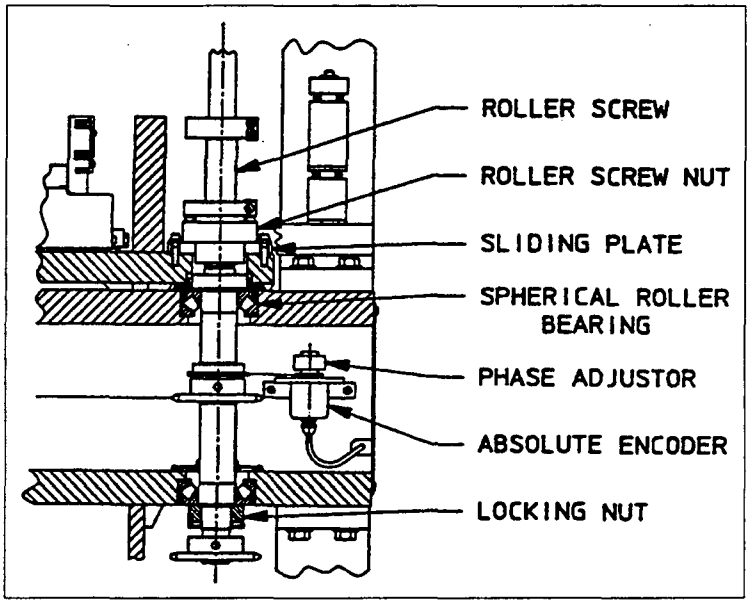

FIG. 24. Transrol roller screw layout.

The roller screws are supported on spherical bearings mounted in the support structure horizontal members. Four right-handed roller screws on the upper section and 4 left-handed roller screws on the lower section, coupled by shaft couplings, and roller chains and sprocket wheels combine to provide equal—but opposite—vertical motion of the upper and lower backing beams. This system is coupled to the gear box by roller chains and sprocket wheels. The stepper motor is connected to the gear box by a flexible coupling.

The drive system has been sized to drive the system under maximum magnetic load (minimum gap), even though compensating springs are used to buck the magnetic load (see Section 5.4.1). The roller screw will have a 2 mm pitch. Since there will be upper and lower roller screws, the total pitch change will be 4 mm per revolution. The gear box has a 30:1 reduction unit. The stepper motor has 200 steps per revolution. A selection of 10 micro-steps/step by the control electronics for the stepper motor will provide 2,000 steps/revolution operation, and result in a gap resolution of 0.07 μm. At 2,000 steps/revolution operation, the motor can easily be driven at a velocity that will move the gap from full closed to full open in approximately 1 minute. The stepper motor is capable of moving the gap for step scans at a 1 bandwidth/second rate. For an 11 cm period insertion device, this translates into a maximum 2.3 mm/second gap change rate.

An absolute encoder is coupled to 1 roller screw shaft by means of a Flex-E-Gear drive with a 4:1.75 step-up ratio. The encoder selected has a resolution of 16,384 word counts per revolution. This combination will read out to a resolution of < 0.1 μm. A harmonic drive phase adjuster is used to calibrate the gap to the encoder readout.

Analysis of the proposed drive system design yields the following: the gap position uncertainty due to stick-slip is < 0.4 μm. Backlash is estimated at 87 μm in gap motion, which requires unidirectional scanning and control of the wiggler gap.[25] With unidirectional scanning, the scan-to-scan gap reproducibility is estimated to be within 11 μm. Calibration tests on the U5.0 Wiggler show gap reproducibility is within ± 5 μm.[26]

Protection for the drive system is as follows:

1. Open-loop control system, with preset limits for travel, stored in the computer program.
2. Micro-switches, for minimum and maximum gap positions, hard-wired to the control system.
3. Mechanical stops for minimum and maximum gap positions.
4. Stepper motor can be stalled at full torque current.
5. Mechanical drive components are designed to handle full stepper motor torque.
6. Full-load current sensing in the control system for shut down after a preset time interval.

5.6.3 System Assembly

The Support/Drive System is assembled first without the magnetic structure installed. It is then disassembled, the magnetic structure installed into backing beams, and the system is reassembled with the vertical magnetic structure installed in the backing beams. This procedure allows for careful alignment of the support and drive systems without the complication of installed magnetic structures.27, 28 Final pinning of the support structure is done after the magnetic measurements are completed. A PIR follows the Support/Drive System assembly and pre-installation work of the wiggler.[29]

Results of tests carried out with the control system on the completed IDB-U5.0 support structure/drive system are tabulated in Table XI, and demonstrates that the system requirements have been met.

Table XI. Support, drive, and control system test results.

Test	Performance
Magnetic structure alignment (upper structure with respect to the lower structure)	Gap parallelism within 5 μm, transverse within 250 μm longitudinal within 150 μm.
Gap range	14 mm to 210 mm
Gap opening-closing time	1 minute
Absolute accuracy	Within ± 5 μm
Backlash (encoder to gap)	Within 10 μm for bidirectional motion
Scan rate	3.33 mm/sec maximum

Magnetic field taper can be provided manually by stepping one of the main roller chain sprockets, with respect to the chain, in increments of 87 μm/sprocket tooth.

5.6.4 Local Temperature Control

It is important that the insertion devices be maintained at a constant temperature during a photon run, typically 8-hour durations. A uniform change in temperature of the device will cause a shift in the energy spectrum. A vertical temperature gradient in the backing beam will cause a broadening of the spectrum.

With a uniform change of 1 degree C in temperature of an insertion device, and operating at small gaps, the energy shift will be 0.2%. With the tunnel air temperature controlled to ± 1 degree C, and the thermal time constant of the magnetic structure at 24 hours, the maximum temperature change that the magnetic structure would experience would be 0.5 degree C in an 8-hour period. This would result in an energy shift of 0.1%, which is acceptable.

Further spectrum shift will occur if the vertical temperature gradient in a backing beam exceeds approximately 0.1 degree C. To prevent a temperature gradient from being established in the backing beam requires that the surrounding air be uniform in temperature. This is accomplished by circulating the air within an insertion device enclosure. Air will be moved with muffin fans, located within the enclosure.

5.7 Insertion Device Control System

The insertion device control system (IDCS) has been designed to provide a general drive system which will accommodate the full compliment of insertions devices at the ALS in terms of accuracy, resolution, speed, and maximum lifting capability. The original requirements were to created a system that could:

— lift an 84,000 pound load,
— transverse 210 mm of gap motion,
— complete a full open-to-close transition in less than 5 minutes,
— absolute positioning accuracy of ± 1 μm,
— minimum scan speed of less than 1.0 mm/sec,
— maximum scan speed greater than 2.31 mm per second, and
— provide a convenient method of controlling the gap position from the control room and experimental stations.

To date, these requirements have been met, with the exception of the ± 1 μm positioning accuracy which is not required for the EW20.0 Elliptical Wiggler with the IDCS.

FIG. 25 presents a schematic of the IDCS, a stepper motor system from Compumotor. To date, 3 identical device control systems have been built for the U5.0 and U8.0 wigglers. The IDCS for the EW20.0 will be identical with these.

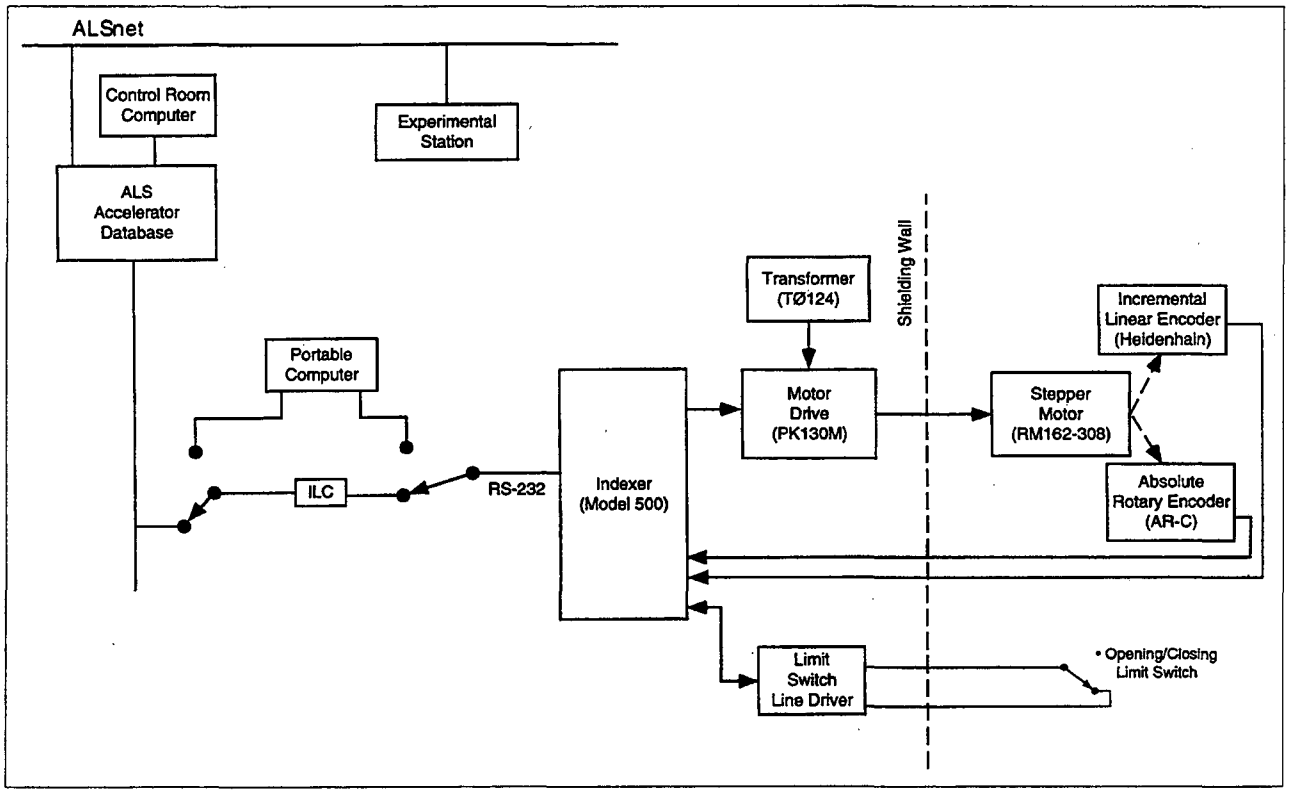

FIG. 25. Insertion device control system.

The motor is capable of micro-stepping at 2,000 steps per revolution, corresponding to 0.0667 μm of gap motion per step, at a maximum velocity of 25 revolutions per second, and corresponding to a gap velocity of 3.33 mm per second. The indexer coordinates the entire drive system. It uses a unique language called "X language" (developed by Compumotor). The system is controlled by sending a sequence of X-language commands to the indexer over an RS-232 connection. This can be done using an ILC, or any other computer with an RS-232 port. The Compumotor AR-C absolute rotary encoder has 16,384 steps per revolution, which corresponds to 0.107 μm of gap motion per step. Using a calibration table, the encoder provides the absolute position of the insertion device gap as well as a software limit switch to protect the vacuum chamber from being punctured by the magnetic pole tips. A second level of protection is provided using micro-switches. If an opening, or closing, limit is detected, the indexer rapidly decelerates the backing beams. If this system fails, then a mechanical hard stop will protect the vacuum chamber.

In order to accurately position the insertion device gap over the 210 mm range of motion, a considerable effort has been spent on the previous undulators in order to understand the drive system behavior. Using the absolute rotary encoder and a finely spaced calibration table, the achieved absolute accuracy of these systems is ± 5 μm. Although the motor drive system is capable of stepping in 0.0667 μm increments, due to the hysteresis and repeatability of the mechanical system, It is difficult to resolve steps less than a few microns. For a 1-micron step size moving unidirectional, one should expect a 0.2 μm error per step.

The insertion device gap position can be easily controlled and monitored from the ALS control room or from the experimental stations via the ALSnet. The user has the options of setting the gap position (mm), gap velocity

(mm/sec), and maximum rate of change of field strength (T/sec). The gap velocity can also be profiled to any desired pattern not exceeding the 2-Hz update rate on velocity change. The gap position is continuously monitored at an approximate 2-Hz update rate. As shown in FIG. 25, one can bypass the main accelerator control system and establish local control at the ILC, or directly at the Indexer, by using a portable computer.

Compensation coils can easily be fitted into the current control system design.

5.8 Vacuum System

The vacuum system for the EW20.0 Elliptical Wiggler includes the elliptical wiggler vacuum chamber, pumping system, vacuum control and diagnostics, transitions, and a support system. A layout of the system is shown in FIG. 26.

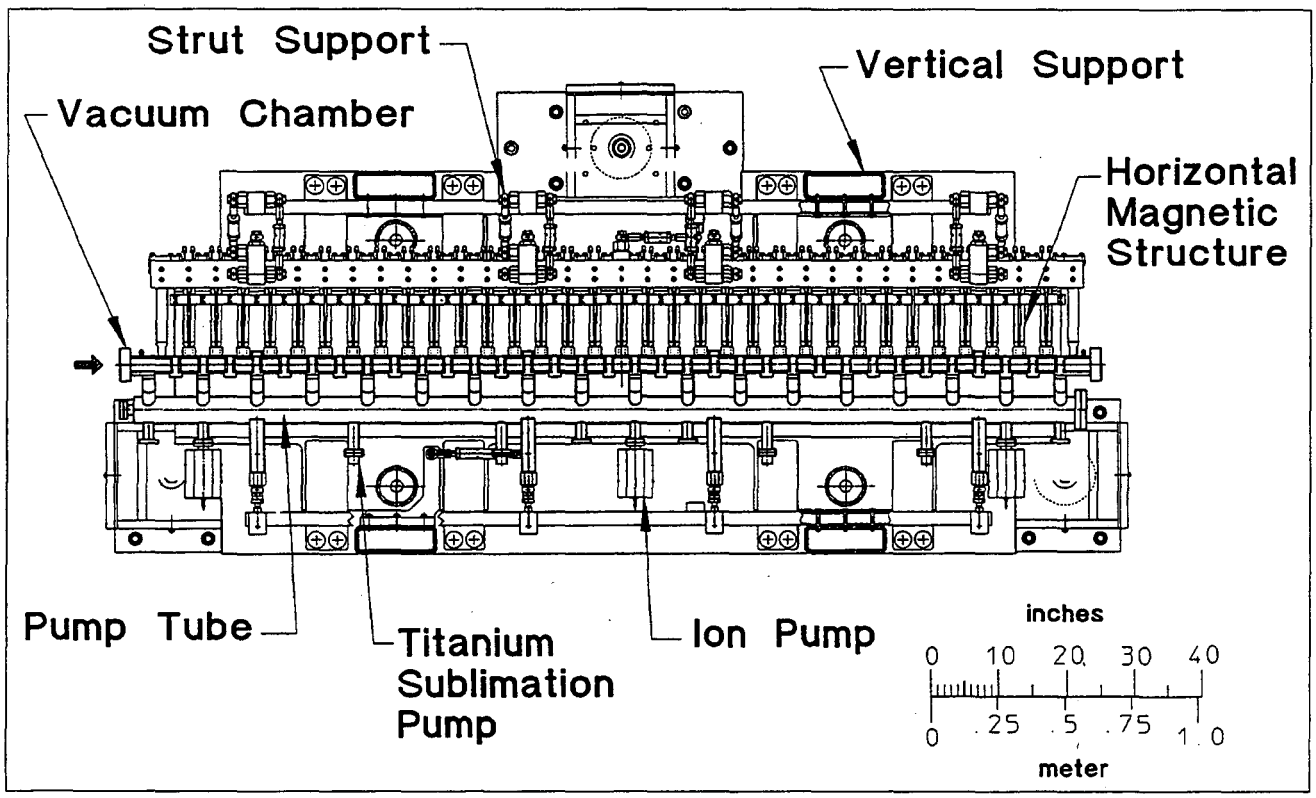

FIG. 26. Vacuum system, plan view.

5.8.1 Vacuum Chamber

The EW20.0 Elliptical Wiggler vacuum chamber is a machined and welded stainless steel assembly that includes a beam chamber, 18 pumpout tubes and a pump tube with appendages for TSP and ion pumps, a roughing valve, an RGA head and diagnostics, as shown in FIG. 27. A cross-section of the chamber is also shown in FIG. 27. The beam chamber aperture vertical dimension of 1.0 cm is based on beam dynamics considerations. The beam chamber horizontal dimension of 6.1 cm minimum is based on a ± 8.82 mrad wiggler fan width.[30] With this beam aperture, a minimum vertical gap of 1.4 cm, and a horizontal magnetic gap of 7.2 cm, are achievable.

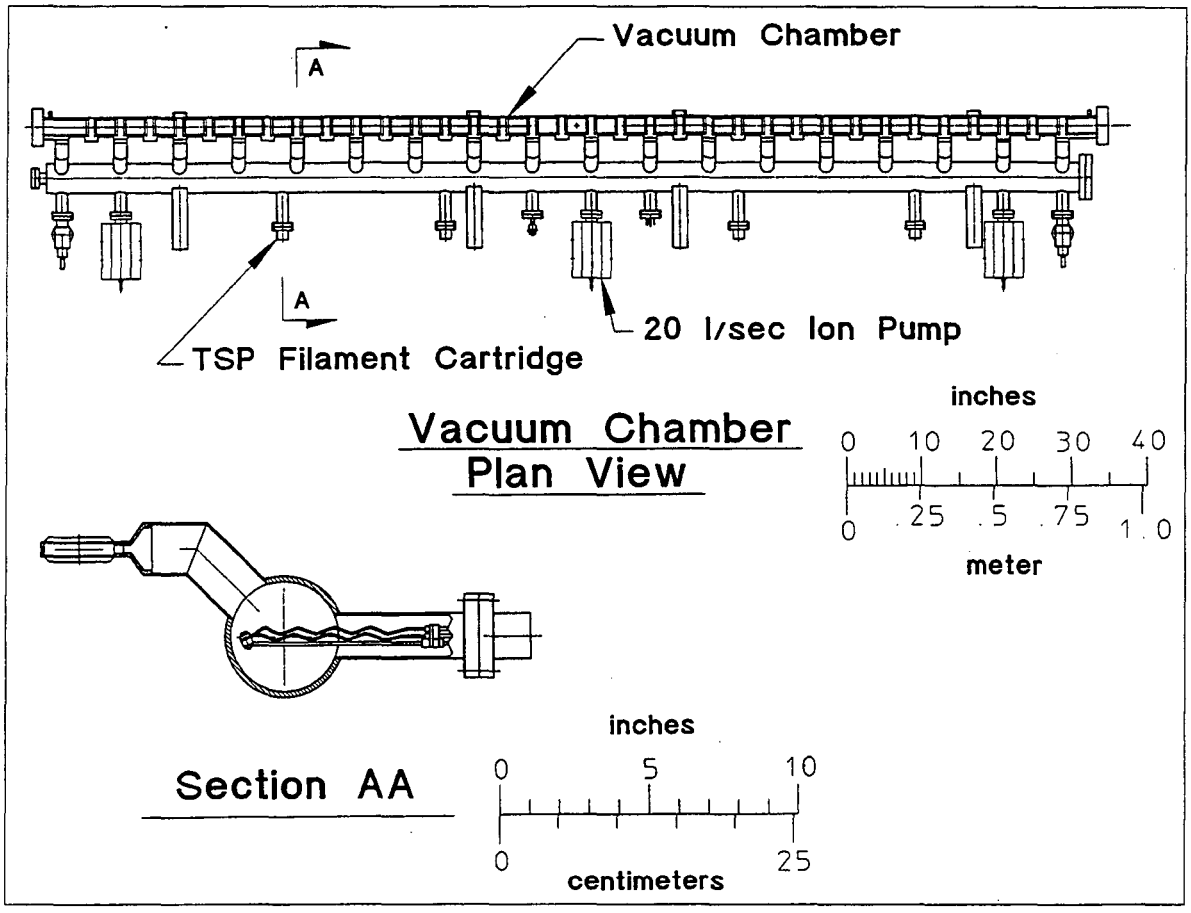

FIG. 27. Vacuum system layout.

Fabrication of this nonmagnetic stainless steel 316 L vessel will be done with a combination of TIG and laser welding techniques. The vertical plates have thin sections, 0.030 inch thick, to allow the vertical magnetic structure poles to achieve the required minimum gap. The horizontal plate, on the side where the synchrotron radiation does not strike, has pumpout openings - one per period. On the other horizontal plate, a rectangular water-cooled channel is provided to remove the heat where some 70 watts of synchrotron light from the upstream bend magnet strikes when the storage ring operates at 1.9 GeV, 400 mA.

Average temperature rise of the chamber is estimated at 1.8 degrees C with the storage ring operating at 1.9 GeV, 400 mA, and with 1 Hz horizontal magnetic-structure operation, which produces only 1 watt of eddy current heating. Peak chamber temperature rise is estimated at 3.4 degrees C. To minimize thermal distortion between the chamber and the adjoining pump tube, the cooling water from the chamber will be ducted to a water circuit attached to the pump tube.

The following tolerance budget described in Table XII shows how the minimum magnetic gap of 14 mm will be achieved with the vacuum chamber.

Table XII. Vacuum chamber tolerance budget.

	mm
Clear aperture of the chamber under vacuum	10.00
Window thickness, 2 x 0.75 mm	1.50
Allowable chamber fabrication flatness, positional, and deflection tolerances	0.95
Installation tolerance (effect of pumps twisting chamber, and alignment)	0.69
Allowable interlock and hard stop allowance	0.86
Minimum EW20.0 magnetic gap	14.00

Under normal operating conditions, photons strike the top and bottom surfaces of the chamber from the last upstream gradient magnet. The heat input to the elliptical wiggler vacuum chamber is less than 1 watt.[31]

The effect of electron beam vertical missteering (during dedicated operation) was examined for the 1.0 cm high aperture vacuum chamber.[32] Allowing the chamber material to approach 80% of yield, 31,000 psi, due to thermal stresses, the maximum allowable vertical missteering angle is ± 0.6 mrad, acceptable since the projected beam would hit the wall of the sector vacuum chamber above, or below, the slot where the insertion device beam exits through the slot.

UHV preparation and bakeout of the chamber will follow a similar procedure, as in previous chambers.[33] Bakeout is at 200 degrees C for a minimum of 48 hours. Typically, a base pressure of less than 3×10^{-10} Torr has been achieved after conditioning.

A 1 m prototype chamber is planned on which welding techniques will be developed and magnetic measurements taken.

The vacuum chamber must be interlocked against low energy storage ring operation with a high field to prevent the wiggler photon beam from impinging on the vacuum chamber.

5.8.2 Pumping System Design

To achieve good vacuum in the presence of the photon induced desorption 18 distributed pumpout ports are located along the length of the beam chamber as shown in FIGS. 26 and 27. To further reduce photon induced desorption, a photon stop is located upstream of the chamber to block some of the beam that would otherwise impinge on the chamber. The pumpout ports are connected to the pump tube to which ion pumps and titanium sublimation filaments are attached. The pumpout ports are slotted to provide satisfactory impedance to the electron beam along the length of the beam chamber. These slots minimally decrease the pumping conductance.

With this combination of pumps, calculations predict that the average pressure distribution should be less than 10^{-9} Torr in the vacuum chamber.[34, 35]

The nominal pumping speeds of the various pumps in the pump tube are tabulated in Table XIII.

Table XIII. EW20.0 vacuum chamber—pumping system speeds.

Pump	Nominal pumping speed (l/s)
20 l/sec ion — 3 units	50
TSP filaments — 4 units	25000

5.8.3 Insertion Device Vacuum Control and Diagnostics

There are 3 - 20 l/s ion pumps on the system. These pumps are driven and monitored by ion pump controllers. The controllers are interfaced to the accelerator control system via the IEEE-488 bus. The titanium sublimation filaments are powered by a single power supply multiplexed to the 4 pumps. The frequency and duration of sublimation will be learned experimentally and controlled by an ILC. It is expected that a few minutes sublimation once a week will be sufficient. Ion pumps and sublimation filaments on the sector arc chambers will be operated in the same fashion.

Monitoring of the ID vacuum chamber pressure is accomplished in 2 ways. The ion pump current is converted to approximate pressure in the local display. A voltage, commensurate with ion pump current, is supplied to the controlling ILC via the bus, then converted to pressure, and presented to the operator as a pressure profile along the insertion device. Accurate pressure measurements in the UHV range are accomplished with nude ion gauges and an ion gauge controller. This controller measures pressure above a millitorr with a thermocouple vacuum gauge. This allows pressure monitoring when the vacuum chamber is being roughed down. An ILC will control and monitor the ion gauge controller via the IEEE-488 bus. This monitoring technique is also used in the sector arc chambers.

5.8.4 Transitions

Storage ring straight sector 11, which includes the elliptical wiggler and the upstream and downstream transitions is shown in FIG. 28. The upstream transition includes the insertion device electron beam position monitors, the storage ring horizontal aperture scrapers, a spool section and a photon stop just upstream of the elliptical wiggler. The downstream section includes a spool section, the storage ring vertical aperture scrapers, and insertion device electron beam position monitors.

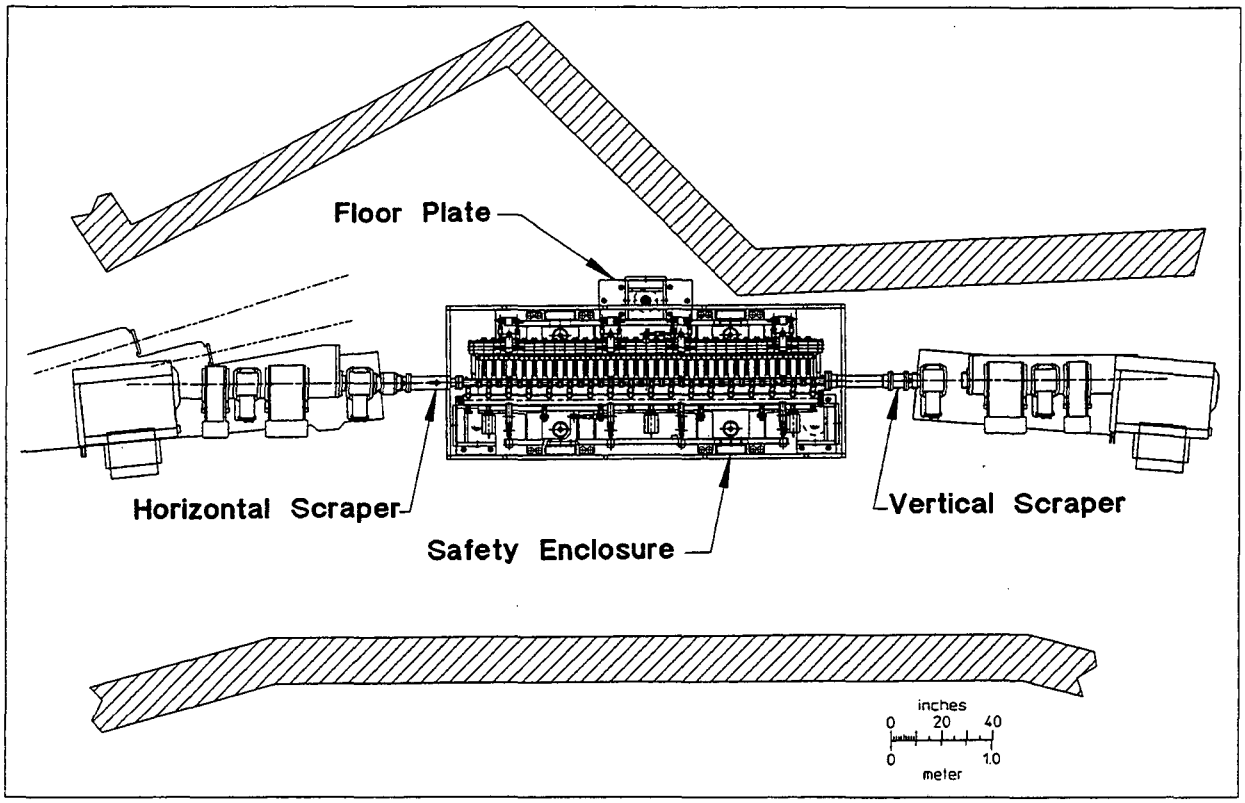

FIG. 28. Elliptical Wiggler installed in storage ring..

Four button electrodes, used to sense the electron beam—similar in design to those in the sector arc chambers—are installed in a symmetrical pattern about the beam centerline at each end of the ID, in the adjacent transition sections, next to the flanges that connect to the ID vacuum chamber. They are shown in LBL Drawing numbers 23L3456 and 23Q4406.

The horizontal and vertical scrapers are modifications of an existing designs shown on LBL Drawing 23Q3496. The photon stop is a similar design to one of the photon stops located in the storage ring RF straight sector, shown on LBL drawing number 23K9016.

5.8.5 Vacuum Chamber and Pumping System Support

For support purposes, the vacuum chamber and pumping system is considered as one assembly. Support of the assembly is accomplished by the use of 2, 6 x 3 inch rectangular, 10-feet-long beams mounted on the upper horizontal beams of the wiggler support structure. The vacuum chamber is supported by eight struts on each side. After final installation, the chamber must be adjusted to be as flat as possible. Additional supports are provided for the ion pump assemblies. The support system is designed to electrically isolate the complete vacuum chamber assembly from the support and drive system and the magnetic structure.

This arrangement, along with the offset pump tube shown in FIG 4., allows the chamber to be lowered in the wiggler and then removed from the device, should the need arise.

5.9 Installation

Installation includes installation of the vacuum system into the elliptical wiggler, preparatory tasks in preparation for the installation of the wiggler, and then the actual installation of the elliptical wiggler into the storage ring.

A plan view of the wiggler installed in the storage ring is shown in FIG. 28.

5.9.1 Vacuum chamber installation

Vacuum chamber installation is as follows:

1. Installation of the vacuum system support structure, which includes installing the 2 large 3.0 m long support beams, the struts, and associated connecting hardware.
2. Surveying and leveling the insertion device, and then determining the vacuum chamber location by survey.
3. Installation of the vacuum chamber, which has been back filled with dry nitrogen into the wiggler with the installation fixture.
4. Installation of the pumping system, then pump down of the system and leak checking.
5. Vacuum system alignment and then the setting of the electrical and mechanical stops.
6. Last, installation of the magnetic shields and the temperature control housing around the wiggler.

5.9.2 Installation Preparation

Tasks required prior to installation include:

1. Surveying the locations of the floor mounting plates in the Storage Ring, core drilling the required holes, and installation of the Hilti anchor studs and floor mount base plates.
2. Surveying the floor mount base plate elevations, determining the kinematic floor mount shim plate thicknesses, fabrication of the shim plates and then installation of the kinematic floor mount shim plates.
3. Installation of cables from the insertion device control system rack to the insertion device in the Storage Ring.
4. Installation of the Horizontal Structure Power Supply, End Structure Power Supplies, and associated cables into the Storage Ring.

5.9.3 Elliptical Wiggler installation into the Storage Ring

Installation requires the following tasks:

1. Remove the Storage Ring shielding in the appropriate straight section.
2. Vent the appropriate Storage Ring section, remove the straight section vacuum chamber, supports, stands and concrete pedestals.
3. Remove the temperature control housing from the wiggler.
4. Prepare the wiggler for transport, unbolt the kinematic mounts (3), lift the wiggler off the kinematic mounts, remove the kinematic mounts (3), and install the kinematic mounts (3) in the appropriate storage ring straight section.
5. Install the inside and outside temperature control housing frames in the Storage Ring.
6. Transport the wiggler to the appropriate Storage Ring Section, install on the kinematic mounts, and bolt down.
7. Remove the hoist equipment from the wiggler and reinstall the Storage Ring shielding.
8. Survey in the wiggler.
9. Take measurements for flex-band installation and carry out the installation of the transitions and flex band.
10. Complete the wiring for the power supplies and control system and check out the system locally.[37]
11. Carry out a UHV bakeout, if required, and activate the TSP pumps.[38, 39]
12. Reinstall the temperature control housing frame, clean the magnetic structure and vacuum system thin-window areas, and install the temperature control housing panels.
13. Verify that the temperature interlock system operates correctly.
14. Checkout the drive system from the control room.[40, 41]
15. Place the wiggler gap in the fully open position and place the wiggler in administrative LOTO.[42]

References

[1] IDH-EW20.0 Cost Estimate, (FY95).

[2] U8.0 Conceptual Design Report, LBL PUB-5276, (May 1990).

[3] S. Marks, Optimization Design Study for ALS Elliptical Wiggler, LSBL Note 207 (July 1994).

[4] K. Halbach, Insertion Device Design: 16 Lectures Presented from October 1988 to March 1989, LBL Publication V 8811-1.1-16.

[5] K. Halbach et al., Error Field Calculation in a Hybrid Insertion Device, (to be published).

[6] R. Schlueter, Engr. Notes, (1994).

[7] W. Hassenszahl, An Assessment of the Effects of Radiation on Permanent Magnet Material in the ALS Insertion Devices, LBL-27808.

[8] D. Humphries, et al., A Multiple Objective Magnet Sorting Algorithm for the ALS Insertion Devices, LBL-35535 (July 1994).

[9] E. Hoyer, 20 cm Period Hybrid Electromagnet Elliptical Wiggler Conceptual Design, (2/92), LBL Engr. Note M7281A, (June 1992).

[10] W16.0 Wiggler Conceptual Design Report, LBL Pub-5288, (February 1991).

[11] E. Hoyer, Magnetic Design, LBL Engr. Note M7479, (February 1995).

[12] K. Halbach, et al., developed PANDIRA, and improved version of POISSON, which allows solution of permanent magnet and residual field problems; POISSON is an improved version of TRIM [A. M. Winslow, J. Computer Phys. 1, 149, (1967)].

[13] TOSCA, an electromagnetic design code by vector fields.

[14] HY3DCM2, a version of Halbach's 3-D hybrid code written by D. Humphries.

[15] E. Hoyer, Multiple Trim Magnets, LBL Engr. Note M7354, (May 1993).

[16] E. Hoyer, Magnetized Neodymium-Iron-Boron Blocks, LBL Specification M802, (April 1994).

[17] E. Hoyer, Backing Beam Deflection, LBL Engr. Note, M7519, (October 1994).

[18] D. Humphries, et al., Precision Alignment of the Advanced Light Source U5.0 and U8.0 Undulators, Proceedings of the SPIE 1993 International Symposium on Optical Applied Science and Engineering, San Diego, California, July 11–16, 1993, LBL-33237.

[19] E. Hoyer, Recommended Standardized Practices for Light Source Magnets, LBL Eng. Note M6711B, (March 1988).

[20] S. Marks, Helmholtz Coil Block Measurement Procedure, ALS Procedure ID-08-02 (March 1994).

[21] S. Marks, et al., Insertion Device Magnet Measurements for the Advanced Light Source, 1993 IEEE-PAC, LBL-33229, (May 1993).

[22] S. Mark, Theory and Design of Halbach Coil for Measurement of Field Integrals at the End of an Insertion Device, LSBL-165 (October 1992).

[23] J. Chin, Site Elevation and Floor Shim Adjustment, LBL Engr. Note M7259, (October 1993).

[24] J. Chin, U8.0 Magnetic Load Compensating Spring, LBL Engr. Note M7228, (September 1993).

[25] J. Chin, Drive System Backlash, LBL Engr. Note M6882, (August 1989).

[26] G. Portman, IDB test result to be published.

[27] J. Chin, Assembly and Alignment Notes, LBL Engr. Note M7349, (September 1993).

[28] J. Chin and W. Gath, Backing Beam Assembly and Alignment Notes, LBL Engr. Note M7435, (October 1993).

[29] J. Chin, Support and Drive System Production/Inspection Record form.

[30] E. Hoyer, Chamber Heating and Heat Transfer, LBL Engr. Note, M7486, (June 1994).

[31] E. Hoyer, Photon Heating of the Undulator Vacuum Chamber, LBL Engr. Note, M6877, (July 1989).

[32] E. Hoyer, Maximum Permissible Vertical Missteering Angle, LBL Engr. Note, M6833, (May 1989).

[33] D. Plate and W. Gath, Insertion Device Vacuum Chamber Bakeout Procedure, LBL Engr. Note M7304, (September 1992).

[34] E. Hoyer, Estimated Vacuum Chamber Gas Load, LBL Engr. Note M7520, (November 1994).

[35] D. Plate, EW20.0 Vacuum System Design Calculations, LBL Eng. Note M7518, (November 1994).

[36] E. Hoyer, Installation of ALS Insertion Devices — IDA, IDB, & IDC Undulators, ALS Procedure ID 02-02, (February 1994).

[37] K. Gershon, G. Portmann, Operating the Installed Insertion Device Motor Control Locally, ALS Procedure ID 02-05, (January 1994).

[38] D. Plate, B. Gath, ALS Procedure ID 02-03, (March 1994).

[39] D. Plate, B. Gath, Activation of NEG and TSP For All ALS Insertion Device Vacuum Systems, LBL Procedure ID 02-04, (February 1994).

[40] J. Young, Testing of Instrument Control Software, ALS Procedure CS 02-02, (October 1993).

[41] G. Portmann, Operating the Insertion Device Gap Motor Control System from the Control Room, ALS Procedure CS 02-03, (October 1993).

[42] J. Chin, E. Hoyer, Undulators IDA, IDB, and IDC Lockout/Tagout (LOTO) Procedure, ALS Procedure ID 09-01, (October 1993).

LAWRENCE BERKELEY LABORATORY
UNIVERSITY OF CALIFORNIA
TECHNICAL AND ELECTRONIC
INFORMATION DEPARTMENT
BERKELEY, CALIFORNIA 94720